

This discussion paper is/has been under review for the journal Atmospheric Chemistry and Physics (ACP). Please refer to the corresponding final paper in ACP if available.

Evaluation of cloud fraction and its radiative effect simulated by IPCC AR4 global models against ARM surface observations

Y. Qian¹, C. Long¹, H. Wang¹, J. Comstock¹, S. A. McFarlane¹, and S. Xie²

¹Atmospheric Sciences and Global Change Division, Pacific Northwest National Laboratory, Richland, WA, USA

²Lawrence Livermore National Laboratory, Livermore, CA, USA

Received: 20 April 2011 – Accepted: 8 May 2011 – Published: 17 May 2011

Correspondence to: Y. Qian (yun.qian@pnl.gov)

Published by Copernicus Publications on behalf of the European Geosciences Union.

Abstract

Cloud Fraction (CF) is the dominant modulator of radiative fluxes. In this study, we evaluate CF simulated in the IPCC AR4 GCMs against ARM ground measurements, with a focus on the vertical structure, total amount of cloud and its effect on cloud shortwave transmissivity. Our intercomparisons of three CF or sky-cover related datasets reveal that the relative differences are usually less than 10 % (5 %) for multi-year monthly (annual) mean values, while daily differences are quite significant. The results also show that the model-observation and inter-model deviations have similar magnitudes for the total CF (TCF) and the normalized cloud effect, and these deviations are twice as large as the deviations in surface downward solar radiation and cloud transmissivity. This implies that other cloud properties, such as cloud optical depth and height, have a similar magnitude of disparity to TCF among the GCMs, and suggests that the better agreement among the GCMs in solar radiative fluxes is the result of compensating errors in cloud vertical structure, cloud optical depth and cloud fraction. The internal variability of CF simulated in ensemble runs with the same model is very minimal. Similar deviation patterns between inter-model and model-measurement comparisons suggest that the climate models tend to generate larger biases against observations for those variables with larger inter-model deviation.

Differences are found in GCM performance over the three ARM sites: Southern Great Plains (SGP), Manus, Papua New Guinea and North Slope of Alaska (NSA). The GCMs perform better at SGP than at the other two sites in simulating the seasonal variation and probability distribution of TCF. However, the models remarkably underpredict the TCF and cloud transmissivity is less susceptible to the change of TCF than observed. Much larger inter-model deviation and model bias are found over NSA than the other sites, suggesting that the Arctic region continues to challenge cloud simulations in climate models. In the tropics, most of the GCMs tend to underpredict CF and fail to capture the seasonal variation of CF at middle and low levels. The high altitude CF is much larger in the GCMs than the observations and the inter-model variability of

Evaluation of cloud fraction and its radiative effect

Y. Qian et al.

Title Page	
Abstract	Introduction
Conclusions	References
Tables	Figures
	
	
Back	Close
Full Screen / Esc	
Printer-friendly Version	
Interactive Discussion	



CF also reaches a maximum at high levels in the tropics, indicating difficulties in the representation of ice cloud associated with convection in the models.

1 Introduction

Three dimensional general circulation models (GCMs) are probably the most powerful tools currently available to quantitatively investigate the Earth climate system and to predict future climate change, which is affected by human activities that cause changes in greenhouse gases, aerosols, and land use and land cover (IPCC, 2007). From a physical point of view, anthropogenic climate change is first of all a perturbation of the Earth's radiation balance (Wild, 2008). Realistic simulation by GCMs of the perturbations of radiation forcing is an important pre-requisite for projecting reliable future climate responses. As Webb et al. (2001) emphasize: "If we are to have confidence in predictions from climate models, a necessary (although not sufficient) requirement is that they should be able to reproduce the observed present-day distribution of clouds and their associated radiative fluxes". Many previous studies have evaluated GCMs' performance in simulating shortwave (SW) and longwave (LW) radiation under cloudy and cloudless skies, both at the surface, where global ground radiation measurement networks are available, and/or at the top of atmosphere (TOA), where satellite observations can be used as constraints (e.g. Garratt, 1994; Wild et al., 1995, 1998, 2008; Li et al., 1997; Walsh et al., 2009). These studies found that GCMs had significant biases and inter-model variability in estimating the SW and LW radiation (Wild and Liepert, 1998; Wild et al., 1999, 2005; Walsh et al., 2009; Wild, 2008). Although in some cases good agreement was found between the observed and modeled cloud radiative forcing, that could be a result of compensating errors in either cloud vertical structure, cloud optical depth or cloud fraction (Potter and Cess, 2004).

The climate science community has identified cloud as one of the highest priorities in climate modeling and climate change projection (IPCC, 2007). Accurate representation of cloud-radiation interaction is critical for climate models to simulate the evolution of the

[Title Page](#)

[Abstract](#)

[Introduction](#)

[Conclusions](#)

[References](#)

[Tables](#)

[Figures](#)

◀

▶

◀

▶

[Back](#)

[Close](#)

[Full Screen / Esc](#)

[Printer-friendly Version](#)

[Interactive Discussion](#)



climate system (Cess et al., 1995). Cloud is also an essential variable in the climate system because it is directly associated with precipitation through its microphysical process and with the aerosol loading through the aerosol aqueous-phase chemistry and wet removal process. Physically, cloud-radiation interactions depend largely on the 5 cloud macrophysical (e.g. cloud fraction, liquid and ice water path) and microphysical (e.g. cloud droplet number, size, and shape) properties. Cloud Fraction (CF) has long been recognized as a dominant modulator of radiation flux at both the surface and the top of the atmosphere (Xi et al., 2010). For example, a 4 % increase in the area of the globe covered by marine stratocumulus clouds would offset the predicted 2–3 K 10 rise in global temperature due to a doubling of atmospheric carbon dioxide (Randall et al., 1984). Although considerable uncertainties are still associated with the cloud feedbacks in GCMs, one can assume that to reasonably simulate future climate, these models should be able to accurately reproduce the current climatology of cloud fraction 15 (including vertical structure) at a given location. The vertical distribution of clouds affects the vertical heating rate profiles through radiative and diabatic processes, and thus influences the atmospheric stratification and general circulation (e.g., Stephens et al., 2002). Recent studies have revealed that the uncertainty in estimating the cloud occurrence at different levels is much larger than in estimating the total cloud amount 20 in most GCMs (Stephens et al., 2002; Zhang et al., 2005; Illingworth et al., 2007; Naud et al., 2008).

Simultaneously evaluating climatological simulations of cloud fraction, especially vertical structure, and radiation in GCMs is difficult because of the lack of a long-term continuous cloud observational dataset. In situ aircraft measurements reveal the macroscopic structure of clouds, but suffer from sampling problems and can only provide 1-D 25 cloud snapshots. Combining aircraft and ground-based instrumentation can provide a more comprehensive view of clouds and their radiative forcing, however the limitations of aircraft campaigns make this possible only for a number of isolated case studies raising the question of representativeness (Illingworth et al., 2007). Remote sensing from space has provided global cloud properties over many years (Rossow and Schiffer,

[Title Page](#)[Abstract](#)[Introduction](#)[Conclusions](#)[References](#)[Tables](#)[Figures](#)[|◀](#)[▶|](#)[◀](#)[▶](#)[Back](#)[Close](#)[Full Screen / Esc](#)[Printer-friendly Version](#)[Interactive Discussion](#)

1991; Webb et al., 2001), but information concerning cloud vertical structure has been lacking (Lin et al., 2006). The recent launch of cloud radar on CloudSat accompanied by the Cloud–Aerosol Lidar and Infrared Pathfinder Satellite Observation (CALIPSO; Winker et al., 2003) provides valuable global cloud information including cloud vertical structure. However, this dataset is still relatively short, and is also limited to only two observational times per day, providing limited information on the diurnal cycle (Wu et al., 2009).

In this study we use simultaneous measurements of cloud fraction and broadband radiation at the surface from the measurement sites operated by the Department of Energy (DOE) Atmospheric Radiation Measurement (ARM) Program (Ackerman and Stokes, 2003). Using radiometers, cloud radar and lidar systems, and other advanced instruments at five permanent sites located in several different climate regimes, ARM provides long-term and nearly continuous observations of the surface SW and LW radiative fluxes, sky cover and cloud vertical distributions. The long-term comprehensive ARM climatological dataset makes it possible to evaluate the CF and surface radiation budgets simulated by GCMs simultaneously, which provides a unique opportunity to study the role of cloud in estimating the surface radiation budgets (Xie et al., 2010). Due to the different scales of the ARM measurements and the GCM simulations, as well as the difficulty in simulating exact weather systems in a free-running GCM, we do not perform direct hour-by-hour or daily comparisons, but instead use the multiple years of ARM data to evaluate the GCMs in a climatological sense.

ARM instruments provide several CF or sky cover related products, such as cloud cover derived from the Total Sky Imager (TSI), Total Sky Cover (TSK) derived from the surface broadband SW radiometers during daytime (Long et al., 2006), effective sky cover (ESK) using broadband LW radiometers during both daytime and nighttime (Long and Turner, 2008), and the frequency of hydrometeor occurrence statistics derived from the narrow field-of-view (FOV) lidar and radar observations (i.e. the Active Remote Sensing of Clouds or ARSCL product, Clothiaux et al., 2000). Before these data can be used to validate GCM cloud statistics, it is necessary to evaluate the measurements

[Title Page](#)

[Abstract](#) [Introduction](#)

[Conclusions](#) [References](#)

[Tables](#) [Figures](#)

[◀](#) [▶](#)

[◀](#) [▶](#)

[Back](#) [Close](#)

[Full Screen / Esc](#)

[Printer-friendly Version](#)

[Interactive Discussion](#)



by these different instruments and to see if they are consistent between themselves at different time scales. Various observational methods and climate models use different definitions for CF (Kassianov et al., 2005). For example, the International Satellite Cloud Climatology Project (ISCCP) defines “total cloud amount” as “the fraction of the earth’s surface covered by cloud” (Hahn et al., 2001). However, in surface climatology studies, it is defined as “the fraction of hemispherical sky covered by cloud” (Hahn et al., 2001). Climate models, on the other hand, typically interpret CF as “the horizontal area fraction covered by clouds as viewed from nadir” (Del Genio et al., 1996). Therefore, comparisons between these FOV and hemispheric observations are important if we want to utilize these data to evaluate climate models.

The aim of the present paper is to evaluate the CF simulations by the GCMs in the 4th assessment report of the Intergovernmental Panel on Climate Change (IPCC AR4, IPCC, 2007), with a focus on the total cloud amount and the vertical structure of CF. Our assessment will seek to identify systematic biases and inter-model deviation in cloud fields simulated in the GCMs across seasonal scales over different regions of the world (e.g. tropics, mid-latitude continent and Arctic). We also discuss how the CF affects cloud transmissivity, a ratio of all-sky mean downwelling SW flux to the cloud-free sky mean, in both observations and GCMs. In the following sessions, we first introduce the IPCC AR4 GCMs and ARM datasets used in the analysis (Sect. 2). In Sect. 3 we compare three CF-related datasets and examine their consistency at different time scales. Then we evaluate the CF simulations in GCMs against the ARM observations, with Sect. 4 focusing on the total cloud amount and cloud transmissivity, and Sect. 5 focusing on the vertical profiles of CF. Summary and discussion are given in Sect. 6. Results of this study will help the climate modeling community to better understand the CF-related measurements from ARM sites and provide useful insights for improving the cloud-radiation interaction and the CF parameterization in climate models.

Evaluation of cloud fraction and its radiative effect

Y. Qian et al.

[Title Page](#)

[Abstract](#)

[Introduction](#)

[Conclusions](#)

[References](#)

[Tables](#)

[Figures](#)

◀

▶

◀

▶

[Back](#)

[Close](#)

[Full Screen / Esc](#)

[Printer-friendly Version](#)

[Interactive Discussion](#)



2 GCMs and ARM datasets

2.1 IPCC AR4 GCMs

The CF and radiative fluxes simulated by more than a dozen GCMs participating in the experiments for IPCC-AR4 are available from the program for climate model diagnosis and inter-comparison (PCMDI). This experimental framework is also known as the World Climate Research Program (WCRP) Coupled Model Intercomparison Project (CMIP3, Meehl et al., 2007). It should be noted that some GCMs archived both total cloud amount and CF at each model layer, but some GCMs only archived total cloud amount. There are also models that did not archive cloud-free sky surface radiation fluxes. For a consistent and fair comparison, we removed some GCMs from the pool. As shown in Table 1, monthly mean CF and surface radiation fluxes from 11 GCMs are used in this study. The 11 models included are from NCAR (model versions cccm3 and pcm1), GFDL (cm2), GISS (e.r), CCSR (MIROC3.2 with high resolution), MRI (cgcm2), UKMO (hadcm3), MPI (echam5), CNRM (cm3), IPSL (cm4) and INM (cm3). The model outputs used in this study are from the AMIP (Atmospheric Model Intercomparison Project) experiment, in which identical observed SSTs were used for all GCMs. 20+ years of results are available approximately from 1980 to 1999, with starting and ending years slightly varied among the models. For more information about these models, the reader is referred to the website of PCMDI (<http://www-pcmdi.llnl.gov/>).

CF is a critical variable in climate models in determining the radiative flux through the atmosphere and at the surface. It is usually parameterized using statistic, diagnostic or prognostic approaches in the models. Table 1 also summarizes the CF parameterization schemes for all GCMs used in this study; for more details including references see http://www-pcmdi.llnl.gov/ipcc/model_documentation/ipcc_model_documentation.php.

Title Page

Abstract

Introduction

Conclusions

References

Tables

Figures

◀

▶

◀

▶

Back

Close

Full Screen / Esc

Printer-friendly Version

Interactive Discussion



2.2 ARM datasets

Evaluation of cloud fraction and its radiative effect

Y. Qian et al.

Our ground observational data are based on the measurements from three permanent ARM sites: the US Southern Great Plains (SGP) at Lamont site, the North Slope of Alaska (NSA) Barrow site, and the Tropical Western Pacific (TWP) Manus site, respectively representing mid-latitude continent, Arctic and tropical climate regions. Conducting the analysis over three very different climate regimes provides better understanding of the geographical variability of cloud and its radiative forcing and a stronger constraint on model simulations. ARM sites are equipped with ground-based active and passive remote-sensing instruments, including the millimeter-wavelength cloud radar (MMCR), the micropulse lidar (MPL), the laser ceilometer, broadband SW and LW radiometers, and the total sky imager (TSI). Through its value-added product (VAP) efforts, ARM has implemented advanced retrieval algorithms and sophisticated objective data analysis approaches to process and integrate data collected from these instruments (Xie et al., 2010). The CF and surface radiation fluxes data are available starting from late 1990s at most of the sites. Approximately 10 yr of valid data are used in this study. More details about ARM data products used in this study can be found at Xie et al. (2010).

At the SGP site, surface radiation flux data are measured by three separate radiometer systems. An ARM Value Added Product called the Best Estimate Flux (the BEF data) (Shi and Long, 2002) combines the measurements from the three systems to produce the best estimate of surface radiation fluxes. For the NSA and TWP sites, the radiation measurements are from the SkyRad and GndRad systems measuring downwelling and upwelling fluxes, respectively. The total downwelling SW fluxes used in this study are primarily the sum of the direct plus diffuse components (measured by Eppley Normal Incidence Pyrheliometer and Eppley shaded Precision Spectral Pyranometers, respectively) whenever available; otherwise the global SW fluxes from the unshaded Eppley Precision Spectral Pyranometers are used. All radiation data used for this study have been quality tested using the QC Rad methodology of Long and Shi (2006, 2008). After the quality tests, data are further processed by the Radiative

Title Page	
Abstract	Introduction
Conclusions	References
Tables	Figures
◀	▶
◀	▶
Back	Close
Full Screen / Esc	
Printer-friendly Version	
Interactive Discussion	



Flux Analysis (RFA). The RFA is a collection of analysis tools that detects clear-sky periods and produces continuous clear (i.e. cloudless) sky estimates of SW fluxes (Long and Ackerman, 2000) and LW fluxes (Long and Turner, 2008) and infers bulk cloud properties such as daylight TSK (Long et al., 2006), ESK (Durr and Philipona, 2004), and cloud effective SW transmissivity from the broadband radiometer data. These measurements have a hemispherical FOV and thus provide time series of fractional sky cover (Kassianov et al., 2005).

By integrating the measurements from the MMCR, MPL and laser ceilometers, the ARSCL product provides an estimate of the total amount and best estimate vertical location of clouds (Clothiaux et al., 1999, 2000). These instruments have a narrow FOV and only detect clouds directly above them. The CF of ARSCL is then derived based on the ARSCL cloud boundary information using the algorithm described in the Climate Modeling Best Estimate (CMBE, Xie et al., 2010 and also at http://science.arm.gov/wg/cpm/scm/best_estimate.html). In this algorithm, a cloud point is first determined by MMCR or MPL and then screened by the best estimate of cloud base from both laser ceilometers and MPL to reduce the problem caused by precipitation in determining cloud base. The ARSCL CF is calculated by averaging the cloud mask points (where cloudy, clear or missing points are set) in a one hour time period. Therefore, the ARSCL CF actually represents the frequency of cloud occurrence rather than cloud fraction. Furthermore, since MMCR cannot separate cloud and precipitation particles throughout the vertical column, the derived ARSCL CF is contaminated by rain particles during precipitation periods, which should be borne in mind in comparing the ARSCL CF with other measurements and model data.

There is occasional missing data in the ARM observations, especially at the remote Manus and NSA sites. In the analysis that follows, we require a 30 % or above of good data for a day or hour to be included in the analysis. For comparisons of two (or three) datasets against each other, we use periods for which all datasets compared have good data. For comparison of a dataset against the GCMs, we include all good data from that dataset, without considering the availability of the other two datasets.

Evaluation of cloud fraction and its radiative effect

Y. Qian et al.

Title Page	
Abstract	Introduction
Conclusions	References
Tables	Figures
	
	
Back	Close
Full Screen / Esc	
Printer-friendly Version	
Interactive Discussion	



3 Inter-comparisons of three ground-based CF related datasets

The ultimate goal of this study is evaluation of GCM simulations of CF and surface radiative fluxes. However, cloud amount can be defined in several different ways. Thus, before presenting the evaluation of the GCM results, we first present inter-comparisons of the three ground-based CF related datasets at different time scales to understand the uncertainties inherent in the observed cloud amount. One definition of cloud amount is the angular amount of the sky dome that is covered by clouds, which is often called the fractional sky cover. The TSI and TSK measurements have hemispheric fields of view and hence are more related to fractional sky cover. In contrast to the sky cover, the earth cover or cloud fraction is defined as the projection of clouds directly down to the surface. The ARSCL CF is derived from the narrow FOV radar and lidar measurements and is simply the percentage of returns that are cloudy within a specified sampling time period. That is, CF is the ratio of the number of 5-min samples when clouds were detected to the total number of 5-min samples when both radar and lidar/ceilometer instruments work. The cloud statistics obtained from such narrow FOV height-time transects might not be representative of a larger area surrounding these instruments at a short time scale (e.g. Berg and Stull, 2002; Kassianov et al., 2005).

To demonstrate the discrepancy between the three datasets on a daily timescale, two time periods are selected here: 29 April to 8 July 2006 and 16 January to 26 March 2007 when all three datasets are available and both MPL and MMCR operate normally in ARSCL. Figure 1 shows the time series of daily total cloud fraction (TCF) based on ARSCL, TSI and TSK over Manus, averaged only for daytime hours between 08:00 to 17:00 (local time). Overall the daytime TCF from ARSCL, TSI and TSK are temporally correlated, especially when TCF is lower (e.g. 1 and 21 June 2006) and/or wind speed is larger (e.g. 1 to 12 February and 28 February to 3 March 2007). However, apparent differences can be found among them, especially between ARSCL and the other two datasets. For example, ARSCL TCF is much larger than TSK and TSI around 22–26 May 2006, as highlighted in top-left panel. This overestimation of TCF by ARSCL is

Evaluation of cloud fraction and its radiative effect

Y. Qian et al.

[Title Page](#)

[Abstract](#)

[Introduction](#)

[Conclusions](#)

[References](#)

[Tables](#)

[Figures](#)

◀

▶

◀

▶

[Back](#)

[Close](#)

[Full Screen / Esc](#)

[Printer-friendly Version](#)

[Interactive Discussion](#)



probably related to persistent cloudiness located directly overhead, as shown in one of the sky images for 24 May 2006 (top-right panel). An opposite case is for 17–18 March 2007, as highlighted in the bottom-left panel, in which the ARSCL underestimates the TCF probably because the clouds are visible, but not directly overhead, as shown on one of the sky images for 17 March 2007 (bottom-right panel). The wind speed is generally less than 2 m s^{-1} for the above two cases, which implies that ARSCL tends to generate larger biases in estimating the TCF as the cloud is slowly moving or stationary, because the one hour temporal average represents a smaller spatial scale during these conditions.

The scatter plots for the daily ARSCL and TSI, ARSCL and TSK, and TSI and TSK values over Manus for days when both datasets are available are shown in Fig. 2. The correlation coefficient between ARSCL and TSI is 0.63, and the root mean square deviation (RMSD) is 0.23, indicating a significant bias (>30 %) between ARSCL and TSI on the daily timescale. There is also a similar significant inconsistency between ARSCL and TSK, with a correlation coefficient of 0.56 and RMSD of 0.24. The correlation coefficient between TSI and TSK is 0.79 and RMSD is 0.17, indicating a relatively smaller bias between TSK and TSI. This is not surprising because ARSCL is derived from the time-slice measurement with narrow lidar/radar FOV, but both TSI and TSK are from hemispheric observations.

There are several possible reasons for the significant bias between the daily TCF from ARSCL and the TSI/TSK measurements. The first possibility is the different fields of view. Although one might expect the TSI/TSK to have a higher CF than ARSCL because the hemispheric FOV instruments will be affected by cloud sides as well as cloud bases, it is also true that the narrow FOV ARSCL instrument samples only a very small fraction of the domain seen by the hemispheric view instruments (TSI and TSK). Thus, if the cloud field is not isotropic, then sampling such a small portion of the cloud field could easily lead to large biases in CF over short time periods. Analysis by McFarlane and Evans (2004) shows that the Nauru cloud field is definitely anisotropic and therefore one would not expect the percentage of clouds seen by the zenith-pointing

Title Page	
Abstract	Introduction
Conclusions	References
Tables	Figures
	
	
Back	Close
Full Screen / Esc	
Printer-friendly Version	
Interactive Discussion	

radar to be the same as the percentage of clouds in a hemispheric field of view. Similar analysis has not been done for the other sites, however, the Nauru site is significantly influenced by the local formation of clouds due to the prevailing wind direction and island heating and there is no indication that the other ARM sites would have similar biases. Pincus et al. (2005) used cloud scenes produced by a 3-D large-eddy simulation model to simulate the CF that would be seen by a vertically pointing narrow FOV instrument and compare it to the model's domain-mean CF. They found that the difference in cloud fraction varied from scene to scene and also depended on the averaging period used, with smaller differences over larger averaging periods.

Another reason for differences in the CF is that the TSI, broadband radiometer, and radar/lidar measurements use very different techniques to detect cloud and thus have different sensitivities to different types of clouds. The MPL instrument, which is included in the ARSCL TCF can detect very optically thin cirrus clouds that may not significantly affect the broadband SW measurements used to determine the TSK cloud amount. The significant bias between narrow FOV and hemispheric observations on a daily basis suggests the users should be extremely cautious to use these datasets to quantitatively evaluate the hourly or daily CF calculated in climate models or retrieved by satellite instruments.

As we are interested in examining the performance of GCMs in a climatological sense, we now examine multiple-year monthly means and annual means of TCF from the three datasets over the sites. There are approximately 10 yr of data available for ARSCL and TSK over these sites. The TSI has fewer years of observations, especially at Manus and NSA. Figure 3 shows the multiple-year averaged monthly mean TCF for ARSCL, TSI and TSK over Manus, SGP and NSA, respectively. The average TCF ranges from 0.65 to 0.85 at Manus, with a minimum value in May. The overall seasonal variability of TCF is small over Manus. Compared to the daily-based TCF, the differences among the three multi-year averaged datasets are much smaller. The annual RMSD between ARSCL and TSI, ARSCL and TSK, TSI and TSK are all less than 0.075, indicating less than 10 % of disagreement among the three multi-year averages.

Title Page	
Abstract	Introduction
Conclusions	References
Tables	Figures
◀	▶
◀	▶
Back	Close
Full Screen / Esc	
Printer-friendly Version	
Interactive Discussion	



Evaluation of cloud fraction and its radiative effect

Y. Qian et al.

Given the large differences in the daily TCF between ARSCL and TSI/TSK, it is somewhat surprising that the monthly differences are less than 10 %. Figure 4 shows the frequency distribution of daily total sky cover or cloud fraction over Manus for multiple years of data. The TSK frequency is larger (smaller) than ARSCL when CF is less (larger) than 0.6. Also the difference between the TSK and ARSCL tends to be significant when CF is larger than 0.8. This is not surprising due to the several orders of magnitude difference in field-of-view between the TSK and ARSCL. During days with large amounts of CF, because of the small sampling of the ARSCL narrow FOV, the ARSCL beam is more likely to be filled with cloud and hence overestimates the TCF. On days with lower cloud cover, the ARSCL beam is more likely to sample clear sky than cloud, and hence underestimates the TCF. The overestimation for larger CF by ARSCL is compensated by less frequent smaller CF, resulting in the small difference among the multi-year monthly mean CFs.

The mean TCF over SGP ranges from 0.35 to 0.62 (Fig. 3b). The overall magnitude of TCF is significantly smaller than over the tropics, although the seasonal variability is greater. The maximum TCF is during winter and spring and the minimum is during July to September. Similar to the results seen at Manus, the monthly mean TCF from ARSCL is larger than that from TSI or TSK, but disagreement among the three datasets is less than 15 %.

The ARSCL TCF ranges from 0.5 to 0.9 at NSA, showing a stronger seasonal variability over the Arctic than at Manus or SGP. TCF increases significantly from March to May (0.5 → 0.8), remains relatively high from May to October except for June and July, and then decreases from October to the next March. The maximum TCF occurs in August–October and the minimum occurs in March. The TSI data is available for fewer years at NSA so is not included in the multiple-year average. TSK measurements are only available from April to September at NSA because they are based on solar radiation. For the available months, the ARSCL and TSK match very well and the difference between them is less than 10 %.

Title Page	
Abstract	Introduction
Conclusions	References
Tables	Figures
◀	▶
◀	▶
Back	Close
Full Screen / Esc	
Printer-friendly Version	
Interactive Discussion	



Table 2 summarizes the annual mean TCF from the different observations and some previous studies over the three sites. The mean TCF over Manus derived from the ARSCL, TSI and TSK is 0.76, 0.74, and 0.71, respectively. We did not find any previous studies that summarized annual mean TCF over Manus. The TCF ranges from 0.45 to 0.51 over SGP, based on this and some previous studies. The TCF from ARSCL in SGP is 0.51 in this study, very close to the values (0.49–0.50) from other studies, including those from synoptic weather stations. The annual TCF based on ARSCL are larger than 0.73 over NSA, which are comparable to those derived from ground-based radar/lidar observations during the Surface Heat Budget of the Arctic Ocean experiment and from satellite observations over the western Arctic regions (Walsh et al., 2009).

Although the point-to-point differences are significant among the three CF datasets on a daily basis, the differences are less than 15 % in the multi-year monthly means and less than 5 % in the annual means over the three sites. The differences in annual mean TCF among ARSCL, TSI, TSK and observation from synoptic weather stations are less than 0.04 (8–9 %) over SGP. Meanwhile, Xi et al. (2010) analyzed one decade of ARM ARSCL and Geostationary Operational Environmental Satellite (GOES) observations at the SGP site and revealed an excellent agreement in the long-term mean CF derived from the surface and GOES data. Dong et al. (2006), Xi et al. (2010), and Kennedy et al. (2010) have also found ARSCL CF to be statistically representative in long-term monthly or annual averages of the entire sky when compared with long-term satellite and surface observations, suggesting that the long-term ARM point observations can represent large areal observations. The consistency between long-term mean narrow FOV, hemispheric and satellite observations provides confidence for using ARM multi-year averaged monthly data to evaluate CF in climate models.

Evaluation of cloud fraction and its radiative effect

Y. Qian et al.

[Title Page](#)

[Abstract](#)

[Introduction](#)

[Conclusions](#)

[References](#)

[Tables](#)

[Figures](#)

◀

▶

◀

▶

[Back](#)

[Close](#)

[Full Screen / Esc](#)

[Printer-friendly Version](#)

[Interactive Discussion](#)



4 Evaluation of surface radiation flux and total cloud amount

4.1 Inter-model divergence and model biases

Wild et al. (1995, 1998, 2005, 2008) have conducted a series of studies evaluating GCMs' performance in simulating solar and LW radiation at surface and top of atmosphere (TOA), under both cloudy and cloudless sky. One of their conclusions is that GCMs tend to generate a larger bias (e.g. too excessive) in estimating the surface insolation than in the net solar fluxes at TOA. This is not so surprising because satellite observed radiation fluxes at TOA are often used as constraints in GCMs. Most current GCMs are tuned to produce correct TOA planetary albedo by adjusting cloud parameters, such as the cloud droplet effective radius used in optical depth calculations and/or the threshold value of autoconversion from cloud to rain. Better performance of GCMs in estimating the radiative fluxes at TOA than at surface suggests that the excessive surface insolation in the GCMs is related to inaccurate partitioning of solar absorption between the surface and atmosphere rather than to excessive absorption by the planet as a whole (Wild et al., 2005).

Here the TCF and the surface SW fluxes simulated in the major GCMs in IPCC-AR4 are inter-compared, and they are also evaluated against ARM measurements over Manus. We compare the SW radiative fluxes under both cloud-free and cloudy skies and also calculate the cloud radiative effects and cloud transmissivity, attempting to investigate the role of TCF and other dimensions of cloud in contributing to the biases of simulated solar radiation fluxes in the GCMs. We find that the performance of GCMs in simulating radiative fluxes is highly related to their simulation of CF. Positive biases in monthly surface downwelling SW flux can be found when the CF is underestimated (figure not shown). However, our focus here is to compare the deviation of 11 GCMs as a group in estimating CF and related radiative effects rather than to examine the performance of each individual model.

Figure 5 compares the aggregate normalized standard deviation (NSD) of annual mean surface downward SW radiation under clear skies (CSWdn) and all-skies

ACPD

11, 14933–14990, 2011

Evaluation of cloud fraction and its radiative effect

Y. Qian et al.

Title Page	
Abstract	Introduction
Conclusions	References
Tables	Figures
◀	▶
◀	▶
Back	Close
Full Screen / Esc	
Printer-friendly Version	
Interactive Discussion	



(SWdn), cloud transmissivity (SWdn/CSWdn, TRANS), TCF (TSK), and cloud effect (CSWdn-SWdn normalized by TCF) over one of TWP sites (Manus) for the 11 GCMs and for the difference between models and measurements, respectively. We define NSD as

$$5 \quad \text{NSD} = \frac{\sqrt{\frac{1}{N} \sum_{i=1}^N (x_i - \bar{x})^2}}{\bar{x}},$$

where x_i represents annual mean value of a variable in a GCM, and N is the number of GCMs used for calculation. \bar{x} represents an observational value or the average of x_i for the 11 models,

$$\bar{x} = \frac{1}{N} \sum_{i=1}^N x_i.$$

- 10 Figure 5a shows that the inter-model NSD for CSWdn is less than 0.02 (2 %), indicating a very small inter-model deviation in estimating the downward solar radiation under cloud-free skies. The model-measurement NSD for CSWdn is also small (less than 0.025), indicating that the models generally do a reasonably good job with surface SW radiation in cloudless skies. The tropical sites examined generally have small aerosol optical depths which may partly contribute to the good agreement between model and measurement for the cloudless sky fluxes.
- 15

- The inter-model NSD for all-sky SWdn is around 0.07, indicating around 4 times larger disparity in the GCMs in estimating the downward solar radiation when clouds are included. The NSD for cloud transmissivity is very close to the value for SWdn, 20 because the deviation in transmissivity is mainly contributed by the SWdn rather than CSWdn. The inter-model NSD for TCF reaches 0.14, twice as large as for SWdn and transmissivity, which indicates the inter-model disparity in TCF is much larger than in downward solar radiation. Meanwhile, the NSD of normalized cloud effect (NCE),

Evaluation of cloud fraction and its radiative effect

Y. Qian et al.

[Title Page](#)

[Abstract](#)

[Introduction](#)

[Conclusions](#)

[References](#)

[Tables](#)

[Figures](#)

◀

▶

◀

▶

[Back](#)

[Close](#)

[Full Screen / Esc](#)

[Printer-friendly Version](#)

[Interactive Discussion](#)



Evaluation of cloud fraction and its radiative effect

Y. Qian et al.

Title Page	
Abstract	Introduction
Conclusions	References
Tables	Figures
	
	
Back	Close
Full Screen / Esc	
Printer-friendly Version	
Interactive Discussion	



defined as $(\text{CSWdn} - \text{SWdn})/\text{TCF}$, shows a similar magnitude of NSD as for TCF, indicating that the other dimensions of cloud besides cloud amount, such as cloud optical thickness and/or cloud height, have a similar magnitude of disparity as TCF within the GCMs. This also suggests that the better agreement among GCMs in the cloudy-sky

5 SW fluxes than in TCF or NCE could be a result of compensating effects from errors in cloud vertical structure, cloud optical depth and/or cloud fraction.

The NSD for model-measurement comparison shows a similar overall pattern to that for inter-model deviation, but the magnitude is larger for all quantities (Fig. 4b). The NSD for CSWdn, SWdn, transmissivity, TCF, and NCE is 0.02, 0.096, 0.092, 0.18 and 10 0.19, respectively, over Manus. The NSD for SWdn and transmissivity is five times as large as for CSWdn, and the NSD for TCF and NCE is twice as large as for SWdn and transmissivity. The similar overall deviation pattern between inter-model and model-measurement comparisons suggests that the climate models tend to generate larger differences against observations for those variables with larger inter-model deviation. 15 The model-measurement NSD values for CSWdn, SWdn, and SWdn/CSWdn are similar at both Manus and Nauru (not shown). The similarity in the agreement in SW fluxes at the two sites coupled with the large difference in TCF and NCE further emphasizes the likelihood of compensating errors in cloud vertical structure, optical depth, and cloud fraction.

20 4.2 Comparison of seasonal cycle of total cloud fraction

The ARM sites represent three different climate regimes, so it is important to evaluate the performance of GCMs in simulating the cloud macrophysical properties over the three different sites. Manus, one of the three TWP sites located in the Western Pacific Warm Pool region, represents a region associated with ENSO that plays a large role 25 in the interannual variability observed in the global climate system. The TWP region consistently has warm sea surface temperatures that produce large surface heat and moisture fluxes into the local atmosphere, causing the formation of deep convective cloud systems and consequent high-altitude cirrus clouds. These cloud systems affect

Evaluation of cloud fraction and its radiative effect

Y. Qian et al.

[Title Page](#)[Abstract](#)[Introduction](#)[Conclusions](#)[References](#)[Tables](#)[Figures](#)[◀](#)[▶](#)[◀](#)[▶](#)[Back](#)[Close](#)[Full Screen / Esc](#)[Printer-friendly Version](#)[Interactive Discussion](#)

the amount of solar energy reaching the surface as well as the amount of heat that can escape into space.

Figure 6 shows comparisons of seasonal TCF for the 11 GCMs and their averages with the three different observations over Manus, SGP and NSA. Clouds at Manus are primarily driven by local convection, although high-level ice clouds are often advected over Manus from convective systems occurring over the Maritime Continent (Mather, 2005). Although overall seasonal variability of TCF is small over Manus, most of the models capture the minimum of TCF during the late spring. Simulated TCFs are more scattered during June to October than other months. While the simulated TCF are very diverse among IPCC AR4 GCMs, the TCF averaged for all the 11 GCMs is close to the measurement in both magnitude and seasonal cycle.

The SGP site is located in north-central Oklahoma, potentially representing the interior regions of many mid-latitude continents, where the clouds are driven by frontal systems or by heating and local convection. The convection is usually short lived over the SGP and does not have the extensive cirrus that is found in the tropics (Mace and Benson, 2008). Shallow cumuli often form in spring and summer under stable synoptic conditions with a strong surface forcing and well-developed boundary layers (Berg et al., 2011). For the long-term average, most of the GCMs (except for one model) well capture the seasonal variation of TCF over the SGP, with a maximum during winter and spring and a minimum during July to September. Compared to the measurements, most of the GCMs underestimate the TCF, so the 11-model average of TCF is consistently smaller than the observations by 0.05–0.1 for almost all months.

Recent studies have demonstrated that the Arctic is more sensitive to climate change than other regions. In particular, the Arctic clouds have long been known to be one of the major sources of uncertainty in simulations of Arctic climate (Randall et al., 1998; Walsh et al., 2005). Cloud cover dominates downward LW radiation that, in turn, strongly influences the initiation and rate of ice/snow melting (Curry et al., 1996). Previous research has estimated that clouds in the Arctic are more prevalent and persistent than clouds elsewhere (Curry et al., 1996). As shown in Fig. 6, the NSA Barrow

site has a relatively large cloud fraction, especially during the warm season in which the low-level cloud is persistent. This persistent large cloud coverage insures its important role in the Arctic climate system. Therefore, it is critical for global climate models to have the right cloud and radiation budget to project future climate change over the 5 Arctic region (Vavrus et al., 2009). Unfortunately, the performance of GCMs is more diverse over NSA than over Manus and SGP, except for August and September. The 11-model averaged TCF is close to the observations, with the exception of months from January to April, during which most of the models overpredict the CF by 0.1–0.2.

4.3 Frequency of occurrence vs. TCF bins

- 10 Figure 7 shows the frequency of occurrence of monthly mean TCF simulated by the 11 GCMs and calculated from observations (TSK) over the three ARM sites. Over Manus (Fig. 7a), the observed TCF shows a narrow nearly normal distribution, with a range from 0.4 to 0.9. Four GCMs, i.e. GISS, CCSM UKMO and CNF-Hires, generally well capture the observed range and PDF pattern of TCF. The PDF pattern from 15 CNRM, GFDL, IPSL is slightly skewed to high TCF compared to the observed nearly normal distribution, indicating a too frequent overprediction with larger cloud cover in those models. Simulated frequency of occurrence in PCM, INM and MPI dramatically increases from lower to higher TCF bins with approximately 60 % of the occurrences having TCF larger than 0.9 in PCM and INM and 45 % of the occurrences having TCF larger than 0.9 in MPI. Apparently too frequent nearly overcast days are simulated over 20 the tropics in these three models. TCF in MRI is almost evenly distributed in bins between 0.1 to 0.8, indicating a too frequent overprediction of low CF and underprediction of larger CF in this model.

Over SGP (Fig. 7b), the observed TCF also shows a near-normal distribution, with the mean about 0.5. The PDF of TCF at SGP has similar shape to the PDF at Manus, but values are shifted to lower bins. A few of the GCMs reasonably capture the near-normal distribution pattern of TCF over SGP, such as IPSL, GFDL, MPI and CNRM. However, the simulated TCF in PCM and UKMO are too evenly distributed over a

Evaluation of cloud fraction and its radiative effect

Y. Qian et al.

[Title Page](#)

[Abstract](#)

[Introduction](#)

[Conclusions](#)

[References](#)

[Tables](#)

[Figures](#)

◀

▶

◀

▶

[Back](#)

[Close](#)

[Full Screen / Esc](#)

[Printer-friendly Version](#)

[Interactive Discussion](#)



Evaluation of cloud fraction and its radiative effect

Y. Qian et al.

bigger range of values. In contrast, TCF is too narrowly distributed in CNF_Hires. This model together with CCSM and GISS all show a shifted TCF distribution to the lower bins, indicating too many cloud-free and/or low cloud-cover days in these three models. Overall the GCMs perform better at SGP than at Manus. This is likely related to the weaker large scale forcing at the TWP compared to SGP, and/or to the more diverse and varying cloud regimes over the tropical region, such as frequent deep convection and cirrus cloud, which are relatively poorly simulated in GCMs.

Over NSA (Fig. 7c), observed TCFs are widely spread in bins between 0.1 and 1.0 but occur more frequently in the higher bins. Except for CNF_Hires, all models tend to show a more narrowly distributed PDF that skews to the higher side of the bins, especially CNRM, INM and MPI, which means too many overcast and/or high cloud-cover days but too few low cloud-cover days in those models. The diversity of model performance in simulating PDF of TCF is also very obvious over NSA, indicating that it remains a significant challenge for GCMs to simulate the right cloud cover over the Arctic region.

4.4 Transmissivity vs. TCF

Not only the total cloud cover but also cloud optical properties influence the amount of SW flux reaching the surface. The absolute impact of the cloud also depends on the magnitude of incoming solar radiation. To characterize the normalized impact of clouds on the surface SW radiation, we use the SW cloud transmissivity (T_{sw} , or $SWdn/CSWdn$). By normalizing by the clear-sky downwelling flux at the surface instead of at the top of the atmosphere, we remove much of the effect of the atmosphere on the surface fluxes so that model treatment of molecular scattering, gaseous absorption, and aerosol is less important to the results (except for potential aerosol indirect effects). The monthly mean SW transmissivity is plotted against the corresponding TCF in Fig. 8 for both the observations and nine GCMs over three ARM sites (the other two GCMs did not archive SW flux under cloud-free skies). Since the SW radiative flux under cloud-free skies (i.e. $CSWdn$) is much better simulated and less scattered among the GCMs (see Fig. 5), the performance of models in estimating the transmissivity



primarily reflects their ability to estimate the cloud influence on the SW flux under all-sky (i.e. SWdn). Figure 8a for Manus shows that the observed transmissivity ranges from 0.5 to 0.9. The observed transmissivity and TCF are highly correlated over Manus, with a correlation coefficient of -0.93. Moreover, the transmissivity almost linearly decreases with increased TCF within the range of observed TCF. The slope of the fitted line (i.e. $s = \Delta T_{SW}/\Delta TCF$) is -0.74, and serves as an indicator of how the aggregate cloud optical properties change with changing cloud amount. For the models, the linear fit slope serves to indicate, given the cloud amounts that the model produces, whether the resultant aggregate cloud optical properties are in line with the observations for that climate regime.

The correlation coefficients between transmissivity and TCF over Manus simulated by the nine GCMs range from -0.74 to -0.96, with most GCMs having less correlation between transmissivity and TCF than seen in the observations. The simulated transmissivity, ranging from 0.4 to 1.0, is overall nominally consistent with the observed. However, the slope (or $\Delta T_{SW}/\Delta TCF$) varies from -0.51 to -0.96, indicating a very wide range of different cloud transmission changes per unit TCF change among the GCMs. For example, the $\Delta T_{SW}/\Delta TCF$ for UKMO and CNF_Hires are -0.51 and -0.52, respectively, and the smallest values among all GCMs. Both these models exhibit an underestimation of TCF (Fig. 6a) with larger transmissivities at the lower TCF range. At the same time, these models overestimate the transmissivity for larger TCF compared to the observations. These differences suggest that the cloud optical thickness is underestimated in these models, resulting in a smaller $\Delta T_{SW}/\Delta TCF$ than observed. The $\Delta T_{SW}/\Delta TCF$ is also underestimated in MRI, which also has too many lower TCF values, and in GFDL, which has too many large TCF occurrences. However, $\Delta T_{SW}/\Delta TCF$ is -0.96 in MPI, which is much higher than the observations or other GCMs. Here again, the MPI TCF frequency is biased toward large TCF, with anomalously high transmissivity for the few occurrences of TCF in the 40–60 % TCF range. This indicates that the transmissivity in MPI is too optically thin for the mid-TCF values, however this is compensated for by the overestimated TCF in MPI (see Fig. 6a) and still results in

Evaluation of cloud fraction and its radiative effect

Y. Qian et al.

[Title Page](#)

[Abstract](#)

[Introduction](#)

[Conclusions](#)

[References](#)

[Tables](#)

[Figures](#)

◀

▶

◀

▶

[Back](#)

[Close](#)

[Full Screen / Esc](#)

[Printer-friendly Version](#)

[Interactive Discussion](#)



Evaluation of cloud fraction and its radiative effect

Y. Qian et al.

Title Page	
Abstract	Introduction
Conclusions	References
Tables	Figures
	
	
Back	Close
Full Screen / Esc	
Printer-friendly Version	
Interactive Discussion	

a reasonable estimation of surface SW flux. Other models show a more reasonable agreement for $\Delta T_{\text{SW}}/\Delta \text{TCF}$ over Manus. The slope of transmissivity against TCF and the correlation coefficients between them for the observations and all GCMs and are summarized in Table 3.

Over SGP, the observed transmissivity ranges from about 0.5 to 0.9, similar to that over Manus and the correlation coefficient between TCF and transmissivity is the same as at Manus. The $\Delta T_{\text{SW}}/\Delta \text{TCF}$ is -0.70 , slightly smaller than at Manus. Except for MRI, all GCMs generally underestimate the $\Delta T_{\text{SW}}/\Delta \text{TCF}$ over SGP (however MRI had a large underestimate of TSW/TCF at Manus). The minimum $\Delta T_{\text{SW}}/\Delta \text{TCF}$ is -0.43 in IPSL, almost 40 % smaller than the observed. As discussed in Sect. 4.2, most of the GCMs significantly underestimate the TCF over SGP. This indicates that current global models tend to remarkably underpredict both TCF and $\Delta T_{\text{SW}}/\Delta \text{TCF}$ over SGP, i.e. cloud cover is smaller and the models tend to generate larger transmissivities at the larger TCF values. For instance, the observations give transmissivity values ranging from 0.5 to 0.7 for TCF from 0.6 to 0.7. Yet the models (except for MRI) range from about 0.6 to 0.7 for the same range of TCF, which then produces the underestimation of $\Delta T_{\text{SW}}/\Delta \text{TCF}$.

Over NSA, a greater variety of $\Delta T_{\text{SW}}/\Delta \text{TCF}$ can be found for both observations and models (Fig. 8c). This is at least in part due to the bi-modal behavior of the relationship for snow covered and non-snow-covered ground. In the snow covered case, multiple reflection of SW between the surface and the clouds increases the SWdn, which increases the SWdn/CSWdn ratio and the ratio then includes not only the actual cloud transmission but also the multiple reflection. The snow covered ground cases are those in the upper right of the observations, with both the snow-covered and non-snow-covered cases producing about the same $\Delta T_{\text{SW}}/\Delta \text{TCF}$ slope. The transmissivity varies from 0.2 to 0.9 in GCMs for TCF larger than 0.9, indicating more divergence in transmissivity and cloud optical thickness under skies with larger cloud fraction. The actual changes are asymptotic with respect to changes in TCF because the cloud optical depths usually tends to increase with increasing cloud fraction.

While a value of -0.71 for the observed $\Delta T_{\text{SW}}/\Delta \text{TCF}$ is close to that at the SGP and Manus sites, the models give very diverse predictions for $\Delta T_{\text{SW}}/\Delta \text{TCF}$, ranging from -0.60 in CNF_Hires to -1.50 in INM. Both $\Delta T_{\text{SW}}/\Delta \text{TCF}$ and TCF (see Fig. 6) are significantly underestimated in CNF_Hires, showing too large transmissivity values for

5 larger TCF in this model. In contrast, $\Delta T_{\text{SW}}/\Delta \text{TCF}$ is overestimated by more than 100 % in the INM, with an attendant lack of smaller TCF values. Seven models overestimate and two models underestimate the $\Delta T_{\text{SW}}/\Delta \text{TCF}$ over NSA, with most models exhibiting little stable correlation between TCF and transmissivity, and thus no well defined bimodal behavior in the relationship. Larger inter-model deviation and model bias against 10 observation over NSA in estimating $\Delta T_{\text{SW}}/\Delta \text{TCF}$ and TCF than other sites suggest that predicting the cloud over the Arctic region is more uncertain and remains a more challenging task for climate modelers.

5 Evaluation of cloud vertical structure

In Sect. 4 we comprehensively evaluated the TCF simulated by IPCC AR4 GCMs and 15 its impact on mean cloud transmissivity and the surface SW flux. However, for climate models, the uncertainty in estimating the cloud occurrence at different levels is likely even larger than the uncertainty in estimating TCF. By comparing the results of 10 GCMs to ISCCP and CERES datasets, Zhang et al. (2005) found that models simulated a four-fold difference in high-top clouds against the observations. Characterizing 20 the vertical distribution of clouds is critical to understanding the physical processes of the feedbacks associated with different types of clouds, because the vertical distribution of clouds affects the vertical heating rate profiles and stratification of the atmosphere. McFarlane et al. (2007) compared cloud vertical structure and radiative heating rates in two versions of the Community Atmosphere Model to ARM observations and 25 found that differences in the vertical structure and optical depth of upper tropospheric ice clouds in the models led to large differences in the radiative heating in the upper troposphere, which could have important implications for tropospheric-stratospheric

[Title Page](#)[Abstract](#)[Introduction](#)[Conclusions](#)[References](#)[Tables](#)[Figures](#)[|◀](#)[▶|](#)[◀](#)[▶](#)[Back](#)[Close](#)[Full Screen / Esc](#)[Printer-friendly Version](#)[Interactive Discussion](#)

dynamics. There are fewer studies that have evaluated the vertical structure of clouds in current GCMs, than the overall cloud radiative forcing, partly because of the lack of reliable long-term observations. Here, we use the long-term ARM observations to do such an evaluation. For simplicity in discussion, low, middle and high clouds are defined as those located at heights of 0–3 km, 3–6 km and higher than 6 km, respectively.

5

5.1 Manus

The simulation of cumulus and stratocumulus in the tropics has been a challenge to the modeling community for a long time (Bretherton et al., 2004). Figure 9a shows the annual mean vertical profiles of cloud fraction (CF) derived from ARM ARSCL observations and simulated by seven GCMs over Manus while Fig. 9b shows the standard deviation among the models. Figure 10 shows the monthly time-height composite plots of CF. Simulated CF in most of the GCMs differs substantially from the observed. Overall, most of the GCMs tend to underpredict CF at low and middle altitudes. For example, the low CF in IPSL, INM, and MRI are less than 4 %, compared to around 10 % of CF in the ARSCL observation. Some of the underprediction of CF at low and middle levels may be due to the fact that it is difficult to screen precipitating clouds out of the ARSCL observations, and the ARSCL CF represents a combination of cloud and precipitation particles. The CCSM is an exception, which significantly overpredicts CF of low and middle clouds. The observation shows a remarkable seasonal variation of CF at different levels (Fig. 10). A minimum CF can be found in April and a maximum one in July at lower levels. Except for CCSM, none of the GCMs capture this seasonal variation of CF at lower levels over Manus.

15

20

25

The high level CF in almost all GCMs is substantially larger than the observation over Manus. The annual mean in some GCMs is 3–4 times larger than the measured. The high level CF averaged in all 7 GCMs is around 3 times as large as that in the ARSCL observation. This is to some extent a result of the coarse vertical resolutions in GCMs, but also of the different thresholds determining thin cloud in climate models and ARM measurements, and of the sensitivity limits of the ARM MMCR and MPL for high

Title Page	
Abstract	Introduction
Conclusions	References
Tables	Figures
	
	
Back	Close
Full Screen / Esc	
Printer-friendly Version	
Interactive Discussion	



Evaluation of cloud fraction and its radiative effect

Y. Qian et al.

altitude clouds. The choice of thresholds in determining thin high-cloud is somewhat arbitrary in climate models or in lidar/radar retrievals. The CF at high altitudes is almost linearly dependent on the cutoff value of the optical thickness of these thin high-clouds. Except for the CCSM, none of the GCMs capture the seasonal variability of CF at high level. The GCMs such as INM and CNF_Hires show no seasonal variation for the high level cloud.

Cloud top in most of the GCMs is notably higher in comparison to the ARSCL observations. The cloud top height is around 17 km in ARSCL, while except for MRI, the cloud top height reaches 19–20 km in most of the GCMs. The cloud top height in ARSCL is probably underestimated to some extent as the radar cannot detect small particles at the top of ice clouds and the lidar is often attenuated in optically thick ice cloud before reaching cloud top. It is interesting that only CCSM can capture the seasonal variability of CF at both low and high levels, although CF in CCSM is larger than the observation at all levels. Meanwhile, the TCF simulated in CCSM is close to that in ARSCL (Tables 2 and 3), which indicates that a different cloud overlap scheme from the true overlap seen in the ARSCL observations is probably used in CCSM. The model-measurement difference reaches a maximum at around 8–16 km, which is also the height that the maximum of inter-model deviation of CF is located. Figure 9b shows that the standard deviation (SD) of CF among the 7 GCMs is larger than 0.15 between 8–16 km, while it is less than 0.1 below 6 km. The larger model-measurement difference and inter-model deviation at higher levels implies the current GCMs have more problems in simulating the high clouds (e.g. cirrus or ice clouds) over the tropic region. Much of the high cloud observed over Manus is outflow from deep convection over the Maritime Continent (Mather, 2005), indicating that the GCMs likely have trouble representing the full radiative impact of tropical deep convection systems. As argued by Waliser et al. (2009), the shortcomings in the representation of these clouds impact both the latent and radiative heating processes, and in turn the circulation and the energy and water cycles, leading to errors in weather and climate forecasts and to uncertainties in quantifying cloud feedbacks associated with global change.

Paper | Discussion Paper | Discussion Paper

Title Page

Abstract Introduction

Conclusions References

Tables Figures

◀ ▶

◀ ▶

Back Close

Full Screen / Esc

Printer-friendly Version

Interactive Discussion



5.2 SGP

Figures 11 and 12 show the annual mean vertical profiles and monthly time-height plots of CF from the ARSCL observation and GCMs over SGP. The observed CF has a bimodal vertical distribution with a higher peak around 6–10 km and a lower one below 2 km. The maximum CF of high clouds occurs during the winter and spring (Fig. 12) when baroclinic wave activity is common over the ARM SGP site (Xi et al., 2010). High-cloud fraction also varies somewhat with the tropopause heights by season due to the change in thermal thickness of the atmosphere. CF is relatively smaller during July to September, especially for low clouds, which is consistent with that for TCF as shown in Fig. 6b.

The GISS and MRI simulate the smallest CF at all levels, while CNF_Hires and INM simulate largest CF at higher level. Most of the GCMs tend to underpredict CF by 50–150 % at low and middle levels. The CF averaged over all GCMs is around half and two-thirds of the values of ARSCL at low and middle levels, respectively. Except for MRI, all other GCMs fail to capture the distinct boundary layer cloud during winter and spring in their simulations. The ARSCL CF at high level is larger than that predicted in the GISS and MRI, but is smaller than that in the other models. The mean CF of all GCMs is only slightly larger than that for the ARSCL observation at high levels. While most of the models capture the minimum CF at low level during July to September, only CCSM relatively reasonably captures the seasonal variation of CF at high level.

While the model-measurement difference is larger at lower level below 5 km, the inter-model deviation of CF is larger for the high cloud (i.e. above 6 km). Figure 11b shows that the SD of CF among the 7 GCMs is around 0.07 between 7–13 km, and is less than 0.03 below 6 km. The SD for both high and low clouds over SGP is only half as large as that over Manus. The smaller inter-model deviation in SGP suggests that the current GCMs perform more consistently in simulating vertical distribution of CF over the mid-latitude continent than the tropic region, which could partly result from the much stronger large scale forcing for SGP compared to the TWP regime.

Evaluation of cloud fraction and its radiative effect

Y. Qian et al.

[Title Page](#)

[Abstract](#)

[Introduction](#)

[Conclusions](#)

[References](#)

[Tables](#)

[Figures](#)

◀

▶

◀

▶

[Back](#)

[Close](#)

[Full Screen / Esc](#)

[Printer-friendly Version](#)

[Interactive Discussion](#)



5.3 NSA

Evaluation of cloud fraction and its radiative effect

Y. Qian et al.

Barrow, the NSA site located at the northernmost location in Alaska, near cryospheric boundaries, has a prevailing east-northeast wind off the Beaufort Sea and is influenced by both extratropical and Arctic synoptic activity (Stone et al., 2002). The observed and simulated annual mean vertical profiles of CF over NSA are shown in Fig. 13. Different from the Manus and SGP, most of clouds in NSA are constrained in a low layer, i.e. below 1–2 km. The CF gradually decreases with the height and the maximum cloud top height is around 10–12 km. Therefore, the total cloud cover is dominated by low clouds over NSA, either single-layered or multilayered systems with a significant low-cloud component. Stammes et al. (1999) found that there is a persistent multilayered cloud regime during summer in the lowest kilometer of the atmosphere where the upper and lower layers appear to be decoupled from each other. The persistence of these multilayered clouds has been attributed to the lack of cloud dissipative processes in the Arctic: precipitation, radiative heating, convective heating of the boundary layer, and/or large-scale synoptic activity. The mechanisms for their multilayered stratification have been proposed by Curry et al. (1996), but more observations are needed for verification. More recently, mixed-phase clouds have been recognized to occur more often than previously assumed, especially during spring and fall (Verlinde et al., 2007).

The observed and simulated monthly mean time-height plots of CF are shown in Fig. 13. The maximum CF of low clouds occurs in late spring characterized by optically thin cloud, late-summer and fall with more optically dense clouds. The deeper boundary layer and low clouds in late summer and fall than in late spring is likely due to the retreat of sea ice from the north coast of Alaska, which increases moisture fluxes into the lower atmosphere. In contrast, the cloudiness in May is typical of continental landmasses in spring (i.e., scattered “fair weather” cumulus clouds that form on an otherwise clear day). In a low-solar-zenith-angle environment such as the Alaskan North Slope, the scattered cumulus clouds sideways scatter a significant fraction of the downwelling solar flux to the surface (Dong et al., 2010).

Title Page	
Abstract	Introduction
Conclusions	References
Tables	Figures
◀	▶
◀	▶
Back	Close
Full Screen / Esc	
Printer-friendly Version	
Interactive Discussion	



While the GCMs generally capture the maximum CF in the boundary layer and vertical variability (i.e. decreasing with height) of CF, some GCMs (e.g. PCM) tend to over-predict the CF at high level and in the boundary layer. It can be found from Figs. 12 and 14 that a fixed cloud top is probably applied in the INM. Figure 13b shows that the SD of CF among the 7 GCMs is around 0.2 near surface and gradually decreases with height. It becomes constant (around 0.05–0.06) between 2–10 km.

5 SD of CF among the 7 GCMs is around 0.2 near surface and gradually decreases with height. It becomes constant (around 0.05–0.06) between 2–10 km.

5.4 Variability among ensemble runs within the same GCM

A few IPCC AR4 models have conducted several ensemble simulations, which is important to identify the internal variability and uncertainty of the model results, especially 10 in projecting the future climate change. For example, GISS has four and IPSL has six ensemble simulations in CMIP3. The modelers usually focus on evaluating the model internal variability and uncertainty for the simulated temperature and precipitation. It will be interesting to examine the internal variability of CF among ensemble simulations.

Figure 15 shows the vertical profiles of CF for four GISS and six IPSL simulations, 15 and their SD among ensemble runs over Manus. The results show that the variability of CF among ensemble runs in the same GCM is minor at all levels. For example, SD for both GISS and IPSL is usually less than 0.005 in Manus, around 2–10 % of inter-model SD. Similar conclusions are found over the SGP and NSA (not shown). This indicates that the internal variability of CF in the same model with ensemble simulations is very 20 small.

6 Summary and discussion

Cloud Fraction (CF) has long been recognized as the dominant modulator of radiative fluxes. In this study, we evaluate CF simulations in the IPCC AR4 GCMs against ARM ground measurements at a climatological time-scale, with a focus on the vertical structure, total amount of cloud and its effect on cloud transmissivity, for both inter-model 25

Y. Qian et al.

[Title Page](#)

[Abstract](#)

[Introduction](#)

[Conclusions](#)

[References](#)

[Tables](#)

[Figures](#)

◀

▶

◀

▶

[Back](#)

[Close](#)

[Full Screen / Esc](#)

[Printer-friendly Version](#)

[Interactive Discussion](#)



deviation and model-measurement discrepancy. The frequency of hydrometeor occurrence statistics derived from the Active Remote Sensing of Clouds (ARSCL) observation, the Total Sky Imager (TSI), and the Total Sky Cover (TSK) derived from surface SW radiometers, all are CF or sky cover related products available at ARM sites. Our intercomparisons reveal that they are correlated with each other but the daily differences are quite significant, suggesting that one should be extremely cautious in using transient CF data to quantitatively evaluate CF calculated in climate models or retrieved by satellite. However, the differences are usually less than 10 % among their multi-year monthly mean values and less than 5 % among their annual mean values, which gives more confidence in using ARSCL CF to evaluate the GCM climatology simulations.

Detailed comparisons of the GCMs results with the ARM observations reveals that the model bias against the observation and the inter-model deviation (disparity) have a similar magnitude for the total CF (TCF) and for the normalized cloud effect, and they are twice as large as that for the surface downward solar radiation and cloud transmissivity. This implies that the other dimensions of cloud, such as cloud optical depth and height, has a similar magnitude of disparity to TCF among the GCMs, and suggests that a better agreement among the GCMs in solar radiative fluxes could be a result from compensating errors in either cloud vertical structure, cloud optical depth or cloud fraction. Similar deviation pattern between inter-model and model-measurement suggests that the climate models tend to generate larger bias against observations for those variables with larger inter-model deviation. The simulated TCF from IPCC AR4 GCMs are very scattered through all seasons over three ARM sites (SGP, Manus and NSA). The GCMs perform better at SGP than at Manus and NSA in simulating the seasonal variation and probability distribution of TCF; however, the TCF in these models is remarkably underpredicted and cloud transmissivity is less susceptible to the change of TCF than the observed at SGP. Much larger inter-model deviation and model bias is found over NSA than other sites in estimating the TCF, cloud transmissivity and cloud-radiation interaction, suggesting that it remains a more challenging task to climate models in predicting clouds over the Arctic region.

[Title Page](#)[Abstract](#)[Introduction](#)[Conclusions](#)[References](#)[Tables](#)[Figures](#)[|◀](#)[▶|](#)[◀](#)[▶](#)[Back](#)[Close](#)[Full Screen / Esc](#)[Printer-friendly Version](#)[Interactive Discussion](#)

Most of the GCMs tend to underpredict CF and fail to capture the seasonal variability of CF at middle and lower levels in the tropics. The high level CF is much higher in the GCMs than the observation and the inter-model variability of CF also reaches maximum at high level in the tropics. Most of the GCMs tend to underpredict the CF by 50–150 % at low and middle levels over SGP. The inter-model deviation for CF is smaller at SGP than Manus, suggesting that the current GCMs perform more consistently in simulating CF over the mid-latitude continent than over the tropic region. Different from clouds over Manus and SGP, most of clouds in NSA are in the lower troposphere. While the GCMs generally capture the maximum CF in the boundary layer and vertical variability, the inter-model deviation is largest near surface over the Arctic. The internal variability of CF simulated in ensemble runs with the same model is very minimal.

While the results in this study could be valuable for advancing our understanding of the CF-related data that are available at ARM sites and for providing insights for the climate modeling community in improving the cloud-radiation interaction and the CF parameterization in climate models, several uncertainties should be taken into account in interpreting the results of this study. The primary one is the cutoff value of the optical depth to define cloudiness in the various observations and climate models. The CF at high altitudes is almost linearly dependent on the cutoff value of the optical thickness of these thin high-clouds. However, the choice of thresholds in determining thin cloud is somewhat arbitrary in climate models and in lidar/radar retrievals. The different cutoff values in defining the clouds in the ARM measurements and in the GCMs could result in an appreciable amount of uncertainties in comparing the CF in the observations and models. It is worth noting that there are on-going efforts to develop cloud radar/lidar simulators that allow simulating the signal that cloud radar/lidar would see in a model-generated world (Marchand et al., 2009). The comparison of clouds between GCMs and ARM observations can be improved once the cloud radar/lidar simulators are implemented into GCMs.

The second uncertainty is related to the different vertical resolutions in the ARSCL

Title Page	
Abstract	Introduction
Conclusions	References
Tables	Figures
	
	
Back	Close
Full Screen / Esc	
Printer-friendly Version	
Interactive Discussion	



dataset and the GCMs. The ARSCL CF is essentially the frequency of occurrence of hydrometeor in each layer with an original thickness of around 45 m, so the values of ARSCL CF would change with the thickness of layers in which the statistics are conducted. Xi et al. (2010) found that the CF at a given altitude increases as the vertical resolution increases from 90 to 1000 m. On the other hand, the GCMs may have different vertical resolutions from one to another and/or from the ARSCL data, which is another uncertainty in comparing the CF simulated by the GCMS to the observations. Different from other atmospheric variables, it may not be appropriate to do simply linear interpolation vertically for the CF because of the complicated overlap issue for clouds.

The third uncertainty is the limited length of the valid measurement data available at the ARM sites. Although the CF and surface radiative fluxes data are available starting from late 1990s in most of sites, less than 10 yr of ARSCL and TSI data are finally used for some variables in this study because of missing data due to instrument down time. However, the surface radiation data are mostly complete, and we show good agreement between the TSI and TSK TCF values, suggesting that the more continuous TSK data are well suited for long term comparison efforts of TCF. Nevertheless, a 20-yr complete dataset would be more ideal for this kind of study in a climatological sense.

It is highly desirable and our original hope to see if the positive and negative attributes of model clouds can be associated with specific physical parameterizations. The results of this study show that there is no particular model with a specific cloud scheme that has superior performance in all aspects of CF simulation than other models in all three sites. The underestimation of TCF and the overestimation of optical thickness of clouds are common over SGP to models that used very different cloud schemes, however, this could be due to completely different reasons. As suggested by Webb et al. (2001), many other model components can be as important as the cloud and precipitation schemes in assessing clouds in models, such as the vertical resolution and cloud microphysical properties. Without carrying out controlled experiments by isolating individual physical parameterization components, it is difficult to pinpoint the source of the model differences.

Title Page	
Abstract	Introduction
Conclusions	References
Tables	Figures
◀◀	▶▶
◀	▶
Back	Close
Full Screen / Esc	
Printer-friendly Version	
Interactive Discussion	



Finally, one future study needed is to evaluate the ARM ground-based vertical CF using satellite cloud data (e.g. CALIPSO), especially for high clouds. While the ARM radar/lidar observations provide the more reliable vertical distributions for CF for verifying the GCM simulations, and Xi et al. (2010) have shown a good agreement in monthly mean CF derived from 10 yr of ARM surface and GOES satellite data, the large-scale satellite data are critical to evaluating GCM simulated spatial distributions of clouds partly because of their much broader spatial coverage and comparable pixel-size to GCM grid-spacing. Certainly the comparisons between the ground- and satellite-based observations must be conducted carefully because of fundamental spatial and temporal differences between the two different observing platforms.

Acknowledgements. The authors acknowledge the support of the Office of Science Biological and Environmental Research (BER) of the US Department of Energy (DOE) as part of the Atmospheric Radiation Measurement (ARM), and Atmospheric Systems Research (ASR) Programs. The Pacific Northwest National Laboratory (PNNL) is operated by Battelle for the DOE under contract DE-AC06-76RLO 1830. Recognition is also extended to those responsible for the operation and maintenance of the instruments that produced the data used in this study; their diligent and dedicated efforts are often underappreciated. This study is also partly supported by the DOE Office of Science (BER)'s Cryosphere Project. Work at LLNL (S. Xie) was performed under the auspices of the US Department of Energy by Lawrence Livermore National Laboratory under contract No. DE-AC52-07NA27344.

References

- Ackerman, T. P. and Stokes, G. M.: The Atmospheric Radiation Measurement Program, *Phys. Today*, 56, 38–44, 2003.
- Berg, L. and Stull, R.: Accuracy of point and line measures of boundary layer cloud amount, *J. Appl. Meteor.*, 41, 640–650, 2002.
- Berg, L. K., Kassianov, E. I., Long, C. N., and Mills Jr., D. L.: Surface summertime radiative forcing by shallow cumuli at the Atmospheric Radiation Measurement Southern Great Plains site, *J. Geophys. Res. D.-Atmos.*, 116, D01202, doi:10.1029/2010JD014593, 2011.

[Title Page](#)[Abstract](#)[Introduction](#)[Conclusions](#)[References](#)[Tables](#)[Figures](#)[Back](#)[Close](#)[Full Screen / Esc](#)[Printer-friendly Version](#)[Interactive Discussion](#)

- Bretherton, C. S., McCaa, J. R., and Grenier, H.: A new parameterization for shallow cumulus convection and its application to marine subtropical cloud-topped boundary layers. Part I: Description and 1D results, *Mon. Weather Rev.*, 132, 864–882, 2004.
- Cess, R. D., Zhang, M. H., Minnis, P., Corsetti, L., Dutton, E. G., Forgan, B. W., Garber, D. P., Gates, W. L., Hack, J. J., Harrison, E. F., Jing, X., Kiehi, J. T., Long, C. N., Morcrette, J. J., Potter, G. L., Ramanathan, V., Subasilar, B., Whitlock, C. H., Young, D. F., and Zhou, Y.: Absorption of solar radiation by clouds: Observations versus models, *Science*, 267, 496–499, 1995.
- Clothiaux, E. E., Moran, K. P., Martner, B. E., Ackerman, T. P., Mace, G. G., Uttal, T., Mather, J. H., Widener, K. B., Miller, M. A., and Rodriguez, D. J.: The Atmospheric Radiation Measurement Program Cloud Radars: Operational Modes, *J. Atmos. Ocean. Technol.*, 16, 819–827, 1999.
- Clothiaux, E. E., Ackerman, T. P., Mace, G. G., Moran, K. P., Marchand, R. T., Miller, M. A., and Martner, B. E.: Objective determination of cloud heights and radar reflectivities using a combination of active remote sensors at the Atmospheric Radiation Measurement Program Cloud and Radiation Test Bed (ARM CART) sites, *J. Appl. Meteor.*, 39, 645–665, 2000.
- Curry, J. A., Rossow, W. B., Randall, D., and Schramm, J. L.: Overview of Arctic cloud and radiation characteristics, *J. Climate*, 9, 1731–1764, 1996.
- Del Genio, A. D., Yao, M. S., Kovari, W., and Lo, K. K. W.: A prognostic cloud water parameterization for global climate models, *J. Climate*, 9, 270–304, 1996.
- Dong, X. Q., Xi, B. K., and Minnis, K.: A Climatology of Midlatitude Continental Clouds from the ARM SGP Central Facility. Part II: Cloud Fraction and Surface Radiative Forcing, *J. Climate*, 19, 9, 1765–1783, 2006.
- Dong, X., Xi, B., Crosby, K., Long, C. N., Stone, R. S., and Shupe, M. D.: A 10 year climatology of Arctic cloud fraction and radiative forcing at Barrow, Alaska, *J. Geophys. Res.*, 115, D17212, doi:10.1029/2009JD013489, 2010.
- Durr, B. and Philipona, R.: Automatic cloud amount detection by surface longwave downward radiation measurements, *J. Geophys. Res.*, 109, D05201, doi:10.1029/2003JD004182, 2004.
- Garratt, J. R.: Incoming shortwave fluxes at the surface – a comparison of GCM results with observations, *J. Climate*, 7, 72–80, 1994.
- Hahn, C., Rossow, W., and Warren, S.: ISCCP cloud properties associated with standard cloud types identified in individual surface observation, *J. Climate*, 14, 11–28, 2001.

[Title Page](#)

[Abstract](#)

[Introduction](#)

[Conclusions](#)

[References](#)

[Tables](#)

[Figures](#)

[◀](#)

[▶](#)

[Back](#)

[Close](#)

[Full Screen / Esc](#)

[Printer-friendly Version](#)

[Interactive Discussion](#)



Illingworth, A. J., Hogan, R. J., O'Connor, E. J., Bouniol, D., Brooks, M. E., Delanoe, J., Donovan, D. P., Gaussiat, N., Goddard, J. W. F., Haeffelin, M., Klein Baltink, H., Krasnov, O. A., Pelon, J., Piriou, J. M., and van Zadelhoff, G. J.: Cloudnet – Continuous evaluation of cloud profiles in seven operational models using ground-based observations, *B. Am. Meteorol. Soc.*, 88(6), 883–895, 2007.

Intergovernmental Panel on Climate Change: *Climate Change 2007: The Physical Science Basis. Contribution of Working Group I to the Fourth Assessment Report of the Intergovernmental Panel on Climate Change*, edited by: Solomon, S., Qin, D., Manning, M., Marquis, M., Averyt, K., Tignor, M., Miller, H. L., and Chen, Z., Cambridge Univ. Press, Cambridge, UK, 2007.

Kassianov, E., Long, C. N., and Ovtchinnikov, M.: Cloud Sky Cover versus Cloud Fraction: Whole-Sky Simulations and Observations, *J. Appl. Meteor.*, 44, 86–98 doi:10.1175/JAM2184.1, 2005.

Kennedy, A. D., Dong, X., Xi, B., Minnis, P., Del Genio, A. D., Wolf, A. B., and Khaiyer, M. M.: Evaluation of the NASA GISS Single-Column Model Simulated Clouds Using Combined Surface and Satellite Observations. *J. Climate*, 23, 5175–5192. doi:10.1175/2010JCLI3353.1, 2010.

Li, Z., Moreau, L., and Arking, A.: On solar energy disposition: a perspective from observation and modeling, *B. Am. Meteorol. Soc.*, 78, 53–70, 1997.

Lin W. Y. and Zhang, M. H.: Evaluation of Clouds and Their Radiative Effects Simulated by the NCAR Community Atmospheric Model Against Satellite Observations, *J. Climate*, 17, 3302–3318, 2004.

Long, C. N. and Shi, Y.: The QCRad Value Added Product: Surface Radiation Measurement Quality Control Testing, Including Climatologically Configurable Limits, Atmospheric Radiation Measurement Program Technical Report, ARM TR-074, 69 pp., available at: <http://www.arm.gov>, 2006.

Long, C. N. and Shi, Y.: An automated quality assessment and control algorithm for surface radiation measurements, *Open Atmos. Sci. J.*, 2, 23–37, doi:10.2174/1874282300802010023, 2008.

Long, C. N. and Turner, D. D.: A method for continuous estimation of clear-sky down-welling longwave radiatiave flux developed using ARM surface measurements, *J. Geophys. Res.*, 113, D18206, doi:101029/2008JD009936, 2008.

Long, C. N., Ackerman, T. P., Gaustad, K. L., and Cole, J. N.: Estimation of Fractional Sky

Evaluation of cloud fraction and its radiative effect

Y. Qian et al.

Title Page

Abstract

Introduction

Conclusions

References

Tables

Figures



Back

Close

Full Screen / Esc

Printer-friendly Version

Interactive Discussion



Evaluation of cloud fraction and its radiative effect

Y. Qian et al.

[Title Page](#)[Abstract](#)[Introduction](#)[Conclusions](#)[References](#)[Tables](#)[Figures](#)[◀](#)[▶](#)[◀](#)[▶](#)[Back](#)[Close](#)[Full Screen / Esc](#)[Printer-friendly Version](#)[Interactive Discussion](#)

- Galin, V., Gates, W. L., Ghan, S. J., Kiehl, J. T., Lacis, A. A., Le Treut, H., Li, Z., Liang, X., McAvaney, B. J., Meleshko, V. P., Mitchell, J. F. B., Morcrette, J. J., Potter, G. L., Rikus, L., Roeckner, E., Royer, J. F., Schlese, U., Sheinin, D. A., Slingo, A., Sokolov, A. P., Taylor, K. E., Washington, W. M., Wetherald, R. T., Yagai, I., and Zhang, M. H.: Intercomparison and interpretation of surface energy fluxes in atmospheric general circulation models, *J. Geophys. Res.*, 97, 3711–3725, 1992.
- Randall, D., Curry, J., Battisti, D., Flato, G., Grumbine, R., Hakkinen, S., Martinson, D., Preller, R., Walsh, J., and Weatherly, J.: Status and outlook for large scale modeling of atmosphere-iceocean interactions in the Arctic, *B. Am. Meteorol. Soc.*, 79, 197–219, 1998.
- Rossow, W. B. and Schiffer, R. A.: ISCCP cloud data products, *B. Am. Meteorol. Soc.*, 72, 2–20, 1991.
- Stamnes, K., Ellingson, R. G., Curry, J. A., Walsh, J. E., and Zak, B. D.: Review of science issues, deployment strategy, and status for the ARM North Slope of AlaskaAdjacent Arctic Ocean climate research site, *J. Climate*, 12, 46–63, 1999.
- Stephens, G. L., Vane, D. G., Boain, R. J., Mace, G. G., Sassen, K., Wang, Z., Illingworth, A. J., O'Conner, E. J., Rossow, W. G., Durden, S. L., Miller, S. D., Austin, R. T., Benedetti, A., and Mitrescu, C.: The cloudsat mission and the A-train, *B. Am. Meteorol. Soc.*, 83, 1771–1790, doi:10.1175/BAMS-83-12-1771, 2002.
- Shi, Y. and Long, C. N.: Best Estimate Radiation Flux Value Added Product: Algorithm Operational Details and Explanations, Atmospheric Radiation Measurement Program Technical Report, ARM TR-008, 58 pp., available at: <http://www.arm.gov>, 2002.
- Stone, R. S., Dutton, E. G., Harris, J. M., and Longenecker, D.: Earlier spring snowmelt in northern Alaska as an indicator of climate change, *J. Geophys. Res.*, 107(D10), 4089, doi:10.1029/2000JD000286, 2002.
- Vavrus, S., Waliser, D., Schweiger, A., and Francis, J.: Simulations of 20th and 21st century Arctic cloud amount in the global climate models assessed in the IPCC AR4, *Clim. Dynam.*, 33(7–8), 1099–1115, doi:10.1007/s00382-008-0475-6, 2009.
- Verlinde, J., Harrington, J., McFarquhar, G., Yannuzzi, V., Avramov, A., Greenberg, S., Johnson, N., Zhang, G., Poellot, M., Mather, J., Turner, D., Eloranta, E., Zak, B., Prenni, A., Daniel, J., Kok, G., Tobin, D., Holz, R., Sassen, K., Spangenberg, D., Minnis, P., Tooman, T., Ivey, M., Richardson, S., Bahrmann, C., Shupe, M., Demott, P., Heymsfield, A., and Schofield, R.: The Mixed-Phase Arctic Cloud Experiment, *B. Am. Meteorol. Soc.*, 88, 205–221, 2007.
- Waliser, D. E., Li, J., Woods, C. P., Austin, R. T., Bacmeister, J., Chern, J., Genio, A. D., Jiang, J.

Evaluation of cloud fraction and its radiative effect

Y. Qian et al.

[Title Page](#)

[Abstract](#)

[Introduction](#)

[Conclusions](#)

[References](#)

[Tables](#)

[Figures](#)

[◀](#)

[▶](#)

[◀](#)

[▶](#)

[Back](#)

[Close](#)

[Full Screen / Esc](#)

[Printer-friendly Version](#)

[Interactive Discussion](#)



- H., Kuang, Z., Meng, H., Minnis, P., Platnick, S., Rossow, W. B., Stephens, G. L., Sun- Mack, S., Tao, W.-K., Tompkins, A. M., Vane, D. G., Walker, C., and Wu, D.: Cloud ice: A climate model challenge with signs and expectations of progress, *J. Geophys. Res.*, 114, D00A21, doi:10.1029/2008JD010015, 2009.
- 5 Walsh, J. E., Vavrus, S. J., and Chapman, W. L.: Workshop on Modeling of the Arctic Atmosphere, *B. Am. Meteorol. Soc.*, 86, 845–852, 2005.
- Walsh, J. E., Chapman, W. L., and Portis, D. H.: Arctic Cloud Fraction and Radiative Fluxes in Atmospheric Reanalyses, *J. Climate*, 22, 2316–2334, doi:10.1175/2008JCLI2213.1, 2009.
- Warren, S. G., Eastman, R. M., and Hahn, C. J.: A survey of changes in cloud cover and cloud types over land from surface observations, 1971–96, *J. Climate*, 20, 717–738, 2007.
- 10 Webb, M., Senior, C., Bony, S., and Morcrette, J.-J.: Combining ERBE and ISCCP data to assess clouds in the Hadley Centre, ECMWF and LMD atmospheric climate models, *Clim. Dyn.*, 17, 905–922, 2001.
- Wild, M.: Discrepancies between model-calculated and observed shortwave atmospheric absorption in areas with high aerosol loadings, *J. Geophys. Res.*, 104, 27361–27371, 1999.
- 15 Wild, M.: Solar radiation budgets in atmospheric model intercomparisons from a surface perspective, *Geophys. Res. Lett.*, 32, L07704, doi:10.1029/2005GL022421, 2005.
- Wild, M.: Short-wave and long-wave surface radiation budgets in GCMs: a review based on the IPCC-AR4/CMIP3 models, *Tellus*, 60A, 932–945, 2008.
- 20 Wild, M. and Liepert, B.: Excessive transmission of solar radiation through the cloud-free atmosphere, *Geophys. Res. Lett.*, 25, 2165–2168, 1998.
- Wild, M., Ohmura, A., Gilgen, H., and Roeckner, E.: Validation of GCM simulated radiative fluxes using surface observations, *J. Climate*, 8, 1309–1324, 1995.
- 25 Wild, M., Ohmura, A., Gilgen, H., Roeckner, E., Giorgetta, M., and Morcrette, J. J.: The disposition of radiative energy in the global climate system: GCM versus observational estimates, *Clim. Dynam.*, 14, 853–869, 1998.
- Winker, D. M., Pelon, J., and McCormick, M. P.: The CALIPSO mission: Spaceborne lidar for observation of aerosols and clouds, *Proc. SPIE*, 4893, 1–11, 2003.
- 30 Wu, D. L., Ackerman, S. A., Davies, R., Diner, D. J., Garay, M. J., Kahn, B. H., Maddux, B. C., Moroney, C. M., Stephens, G. L., Veefkind, J. P., and Vaughan, M. A.: Vertical distributions and relationships of cloud occurrence frequency as observed by MISR, AIRS, MODIS, OMI, CALIPSO, and CloudSat, *Geophys. Res. Lett.*, 36, L09821, doi:10.1029/2009GL037464, 2009.

[Title Page](#)[Abstract](#)[Introduction](#)[Conclusions](#)[References](#)[Tables](#)[Figures](#)[◀](#)[▶](#)[◀](#)[▶](#)[Back](#)[Close](#)[Full Screen / Esc](#)[Printer-friendly Version](#)[Interactive Discussion](#)

Evaluation of cloud fraction and its radiative effect

Y. Qian et al.

Xi, B., Dong, X., Minnis, P., and Khaiyer, M. M.: A 10 year climatology of cloud fraction and vertical distribution derived from both surface and GOES observations over the DOE ARM SPG site, *J. Geophys. Res.*, 115, D12124, doi:10.1029/2009JD012800, 2010.

Xie, S., McCoy, R., Klein, S. A., Cederwall, R. T., Wiscombe, W. J., Clothiaux, E. E., Gaustad, K. L., Golaz, J. C., Hall, S., Jensen, M., Johnson, K. L., Lin, Y., Long, C. N., Mather, J. H., McCord, R. A., McFarlane, S. A., Palanisamy, G., Shi, Y., and Turner, D. D.: ARM Climate Modeling Best Estimate Data – A new data product for climate modelers, *B. Am. Meteorol. Soc.*, 91(1), 13–20, doi:10.1175/2009BAMS2891.1, 2010.

Zhang, M. H., Lin, W. Y., Klein, S. A., Bacmeister, J. T., Bony, S., Cederwall, R. T., Del Genio, A. D., Hack, J. J., Loeb, N. G., Lohmann, U., Minnis, P., Musat, I., Pincus, R., Stier, P., Suarez, M. J., Webb, M. J., Wu, J. B., Xie, S. C., Yao, M. S., and Zhang, J. H.: Comparing clouds and their seasonal variations in 10 atmospheric general circulation models with satellite measurements, *J. Geophys. Res.*, 110, D15S02, doi:10.1029/2004JD005021, 2005.

[Title Page](#)[Abstract](#)[Introduction](#)[Conclusions](#)[References](#)[Tables](#)[Figures](#)[Back](#)[Close](#)[Full Screen / Esc](#)[Printer-friendly Version](#)[Interactive Discussion](#)

Table 1. A summary of cloud fraction scheme and data availability in IPCC AR4 GCMs used in this study.

Model ID	Model Short Name	Cloud Scheme	References	Total Cloud Amount	Layer Cloud Fraction	All-sky SFC downward SW	Clear-sky SFC downward SW
CCSM3 (USA)	ccsm	Prognostic cloud condensate with diagnostic cloud amount	Rasch and Kristjansson (1998) Zhang et al. (2003) Boville et al. (2006)	✓	✓	✓	✓
CNRM-CM3 (France)	cnrm	Statistical cloud cover scheme for stratiform clouds; Convective cloud cover based on mass-flux transport	Ricard and Royer (1993)	✓		✓	✓
IPSL-CM4 (France)	ipsl	Diagnostic CF based on log-normal PDF of total water	Bony and Emmanuel (2001)	✓	✓	✓	✓
ECHAM5/MPI-OM (Germany)	mpi	Prognostic water phases; Bulk cloud microphysics; Relative Humidity based CF scheme	Lohmann and Roeckner (1996) Roeckner et al. (2003)	✓		✓	✓
GFDL-CM2.0 (USA)	gfdl	Cloud microphysics after Rotstain, 2000; Prognostic CF after Tiedtke, 1993.	Rotstain (2000) Tiedtke (1993)	✓		✓	✓
GISS-ER (USA)	giss	Prognostic cloud condensate with diagnostic CF based on RH above a tunable RH threshold	Del Genio et al. (1996) Sundqvist et al. (1989) Schmidt et al. (2005)	✓	✓	✓	✓
INM-CM3.0 (Russia)	inm	Diagnostic CF; Stratiform CF: linear function of RH; Convective CF is 0.5 for shallow and depends on precip. for deep convection	Alekseev et al. (1998)	✓	✓	✓	✓
MIROC3.2 (hires) (Japan)	cnf_hires	Prognostic cloud water and statistical large-scale CF scheme	Le Treut and Li (1991)	✓	✓	✓	✓
MRI-CGCM2.3.2 (Japan)	mri	Diagnostic cloud water based on T. Diagnostic CF based on RH, separately for convective vs layer and land vs ocean.	Yukimoto et al. (2001)	✓	✓	✓	✓
PCM (USA)	pcm	Diagnostic cloud condensate and cloud cover	Kiehl et al. (1998)	✓	✓	✓	
UKMO-HadGEM1 (UK)	ukmo	Diagnostic with triangular PDF; Parameterized critical RH and a vertical gradient cloud scheme	Smith (1990) Cusack et al. (1999) Smith et al. (1999)	✓		✓	✓

Evaluation of cloud fraction and its radiative effect

Y. Qian et al.

[Title Page](#)

[Abstract](#)

[Introduction](#)

[Conclusions](#)

[References](#)

[Tables](#)

[Figures](#)



[Back](#)

[Close](#)

[Full Screen / Esc](#)

[Printer-friendly Version](#)

[Interactive Discussion](#)



Evaluation of cloud fraction and its radiative effect

Y. Qian et al.

Table 2. Annual mean Total Cloud Fraction (TCF) over three sites.

Site	ARSCL	TSI	TSK	ARSCL or other instruments			
Manus	0.76	0.74	0.71				
SGP	0.51	0.45	0.47	0.47 ¹	0.49 ²	0.49 ³	0.50 ⁴
NSA	0.73		0.77 ⁶	0.78 ⁷	0.75 ⁸		

¹ ARM SGP Radar-lidar, 1997–2006, Table 2 in Xi et al. (2010).

² ARM SGP Radar-lidar, 1997–2002, Dong et al. (2006).

³ ARM SGP ARSCL, 1998–2004, Kollia et al. (2007).

⁴ Global 5° × 5° Surface observation from synoptic weather stations for 1971–1996, Warren et al. (2007).

⁵ Surface observation from two synoptic weather stations nearby SGP for 1981–1991, Lazarus et al. (2000).

⁶ Only averaged from April to September.

⁷ ARM NSA Radar-lidar, Table 2 in Dong et al. (2010).

⁸ ARM NSA Ceilometer, Table 2 in Dong et al. (2010).

- [Title Page](#)
- [Abstract](#) | [Introduction](#)
- [Conclusions](#) | [References](#)
- [Tables](#) | [Figures](#)
- [◀](#) | [▶](#)
- [◀](#) | [▶](#)
- [Back](#) | [Close](#)
- [Full Screen / Esc](#)
- [Printer-friendly Version](#)
- [Interactive Discussion](#)



Evaluation of cloud fraction and its radiative effect

Y. Qian et al.

Table 3. Slope and correlation coefficient (in parentheses) between cloud cover and cloud transmissivity based on ARM data and nine GCMs results over three ARM sites.

	Manus	SGP	NSA
ARM	-0.74(-0.93)	-0.70(-0.93)	-0.71(-0.87)
crrm	-0.71(-0.75)	-0.58(-0.90)	-0.76(-0.66)
gfdl	-0.64(-0.79)	-0.58(-0.88)	-0.84(-0.54)
ccsm	-0.78(-0.82)	-0.59(-0.83)	-1.25(-0.77)
inm	-0.81(-0.74)	-0.57(-0.85)	-1.50(-0.86)
ipsl	-0.80(-0.76)	-0.43(-0.90)	-0.69(-0.64)
cnf_h	-0.52(-0.85)	-0.51(-0.82)	-0.60(-0.92)
mpi	-0.96(-0.86)	-0.56(-0.79)	-0.96(-0.79)
ukmo	-0.51(-0.84)	-0.66(-0.97)	-0.89(-0.92)
mri	-0.63(-0.96)	-0.77(-0.96)	-1.15(-0.88)

Title Page	
Abstract	Introduction
Conclusions	References
Tables	Figures
◀	▶
◀	▶
Back	Close
Full Screen / Esc	
Printer-friendly Version	
Interactive Discussion	



Evaluation of cloud fraction and its radiative effect

Y. Qian et al.

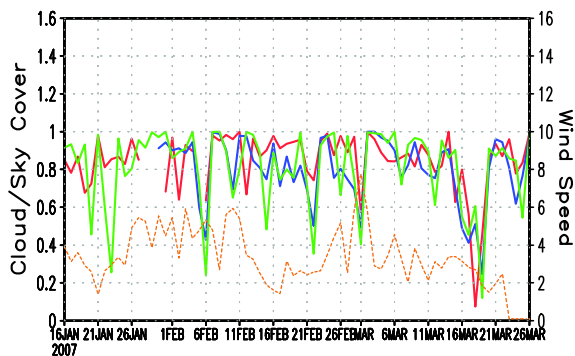
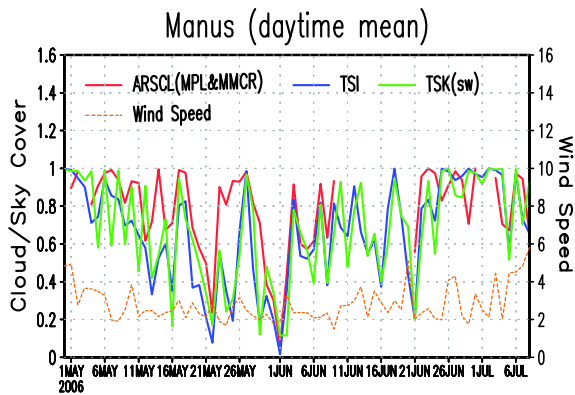


Fig. 1. The time series of daily total sky cover or cloud fraction based on ARSCL, TSI and TSK over Manus, averaged only for daytime hours for 29 April to 8 July 2006 (top) and 16 January to 26 March 2007 (bottom), respectively, when all three datasets are available and both MPL and MMCR operate normally in ARSCL. Right panels are corresponded total sky images.

[Title Page](#)

[Abstract](#)

[Introduction](#)

[Conclusions](#)

[References](#)

[Tables](#)

[Figures](#)

[◀](#)

[▶](#)

[◀](#)

[▶](#)

[Back](#)

[Close](#)

[Full Screen / Esc](#)

[Printer-friendly Version](#)

[Interactive Discussion](#)

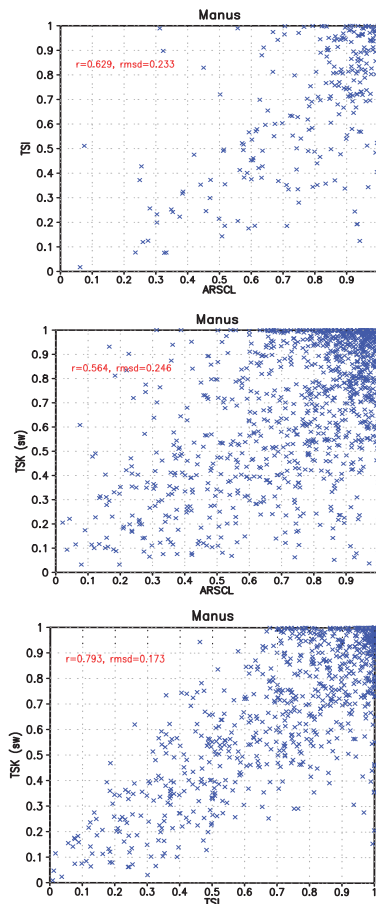


Fig. 2. The scatter plots for daily total sky cover or cloud fraction based on ARSCL and TSI (top), ARSCL and TSK (middle), and TSI and TSK (bottom) over Manus.

Evaluation of cloud fraction and its radiative effect

Y. Qian et al.

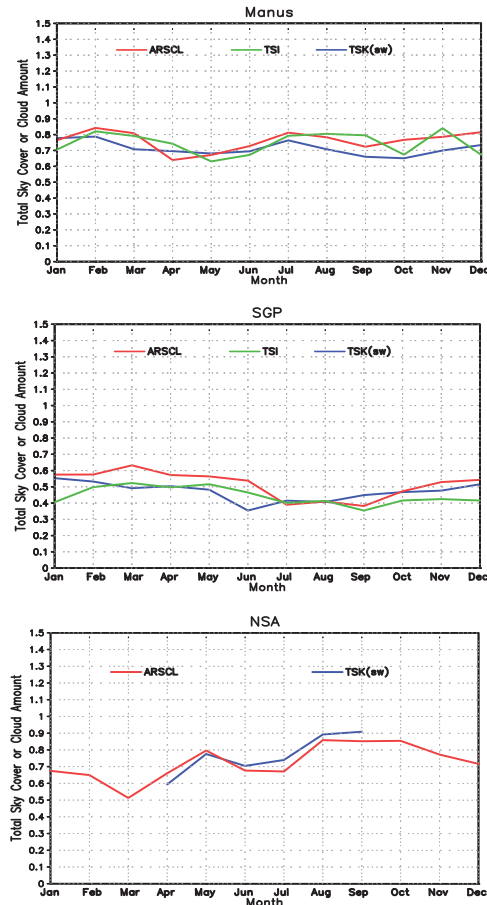


Fig. 3. The multiple-year averaged monthly mean total sky cover or cloud fraction from ARSCL, TSI and TSK over Manus (top), SGP (middle) and NSA (bottom), respectively.

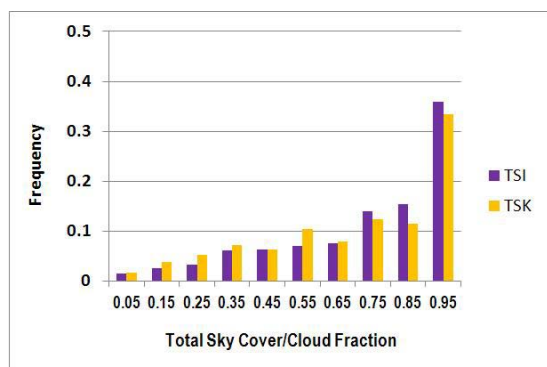
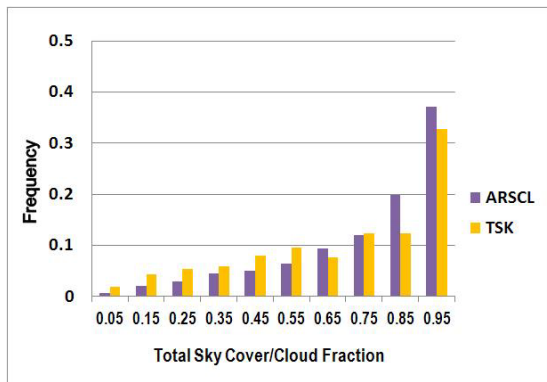


Fig. 4. The frequency distribution for daily total sky cover or cloud fraction over Manus (Top: ARSCL and TSK; Bottom: TSI and TSK).

Evaluation of cloud fraction and its radiative effect

Y. Qian et al.

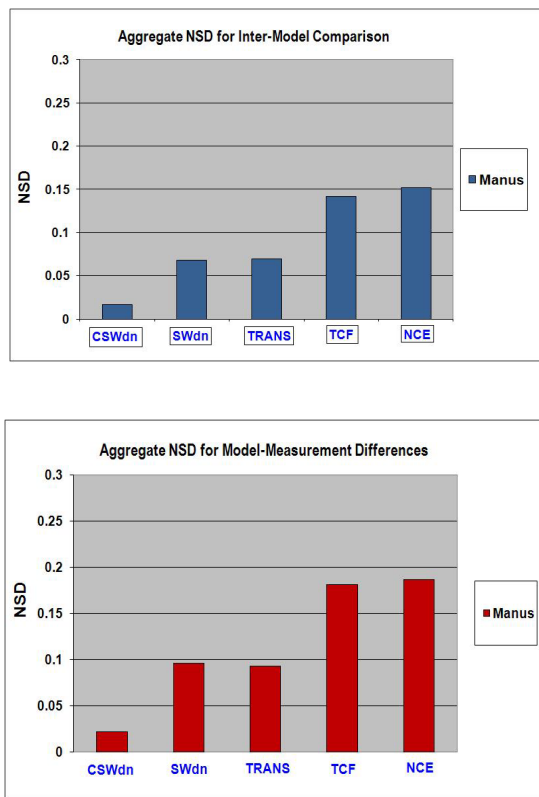


Fig. 5. The aggregate normalized standard deviation (NSD) of annual mean surface downward solar radiation under cloud-free skies (CSWdn) and all-skies (SWdn), cloud transmissivity (TRANS, SWdn/CSWdn), total cloud fraction (TCF), and cloud effect (NCE, CSWdn-SWdn normalized by TCF) over Manus, for inter-model comparison within 11 GCMs (top) and model-measurement difference (bottom), respectively.

Evaluation of cloud fraction and its radiative effect

Y. Qian et al.

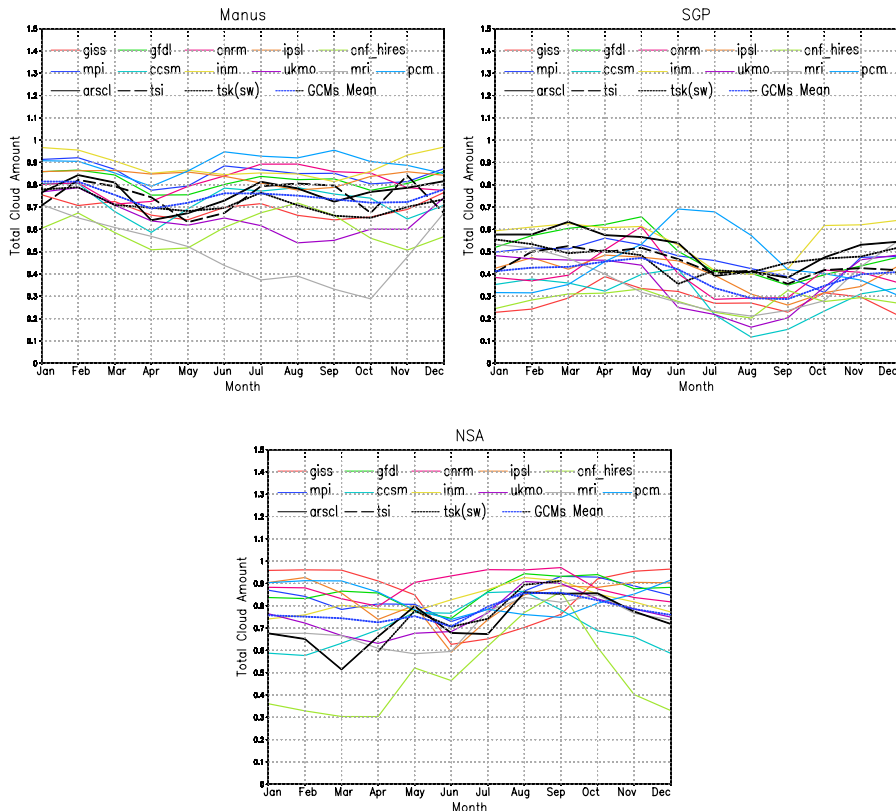


Fig. 6. The multi-year averaged monthly mean TCF for 11 GCMs and their average against three different observations over Manus (top), SGP (middle) and NSA (bottom).

[Title Page](#)

[Abstract](#)

[Introduction](#)

[Conclusions](#)

[References](#)

[Tables](#)

[Figures](#)



[Back](#)

[Close](#)

[Full Screen / Esc](#)

[Printer-friendly Version](#)

[Interactive Discussion](#)

Evaluation of cloud fraction and its radiative effect

Y. Qian et al.

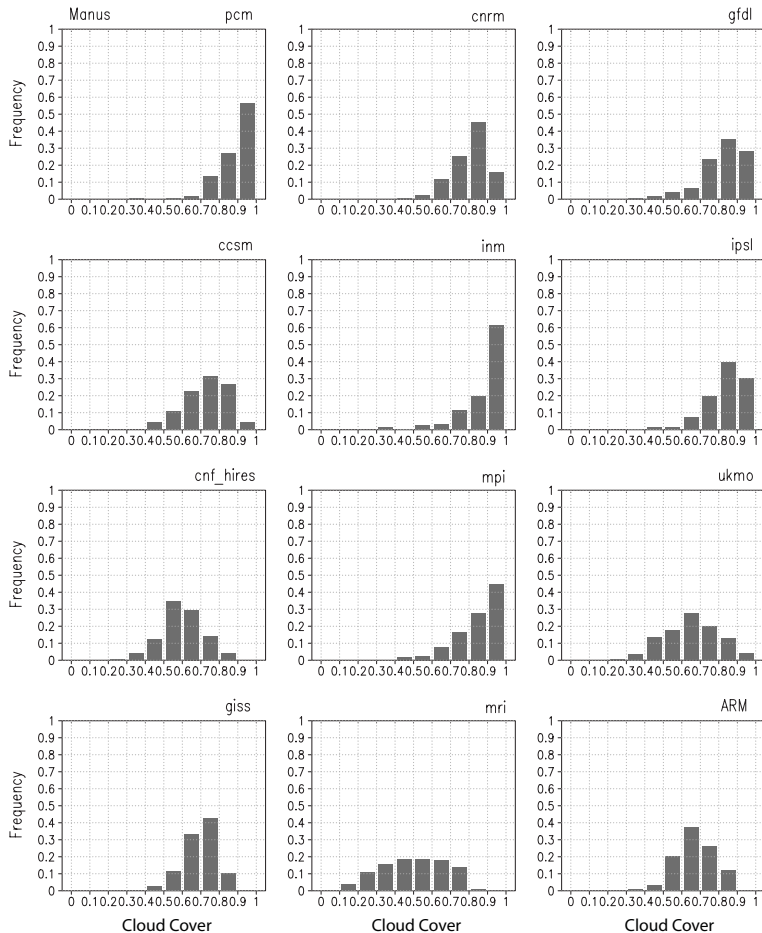


Fig. 7a. The frequency of occurrence (PDF) of monthly mean TCF simulated by 11 GCMs and calculated from observation over three ARM sites. **(a)** Manus, **(b)** SGP, and **(c)** NSA.

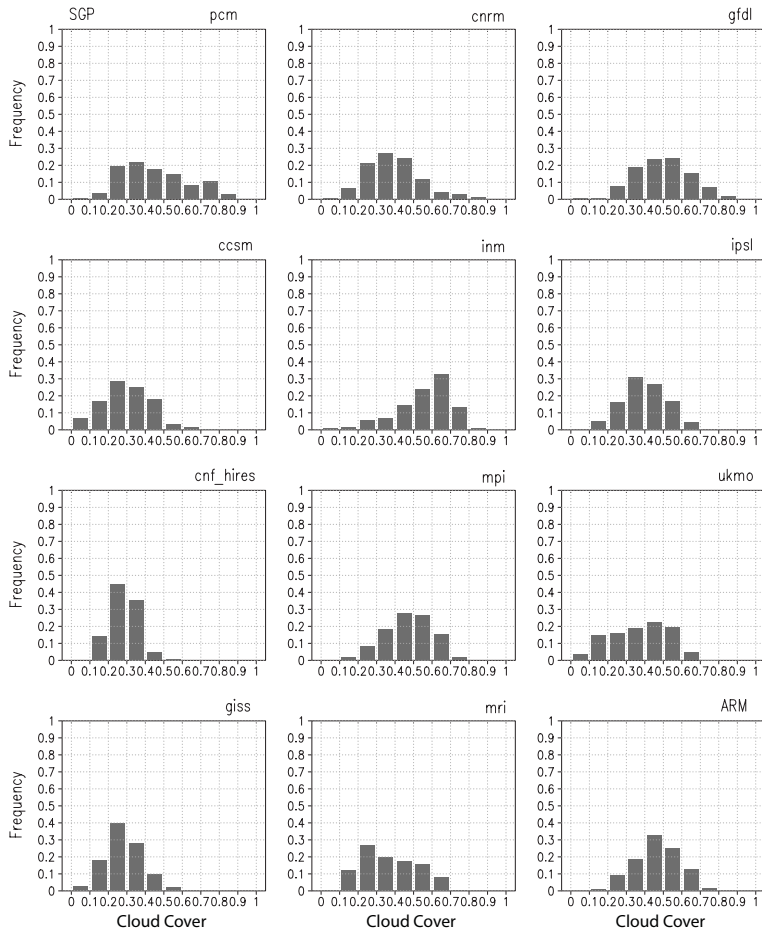


Fig. 7b. Continued.

Evaluation of cloud fraction and its radiative effect

Y. Qian et al.

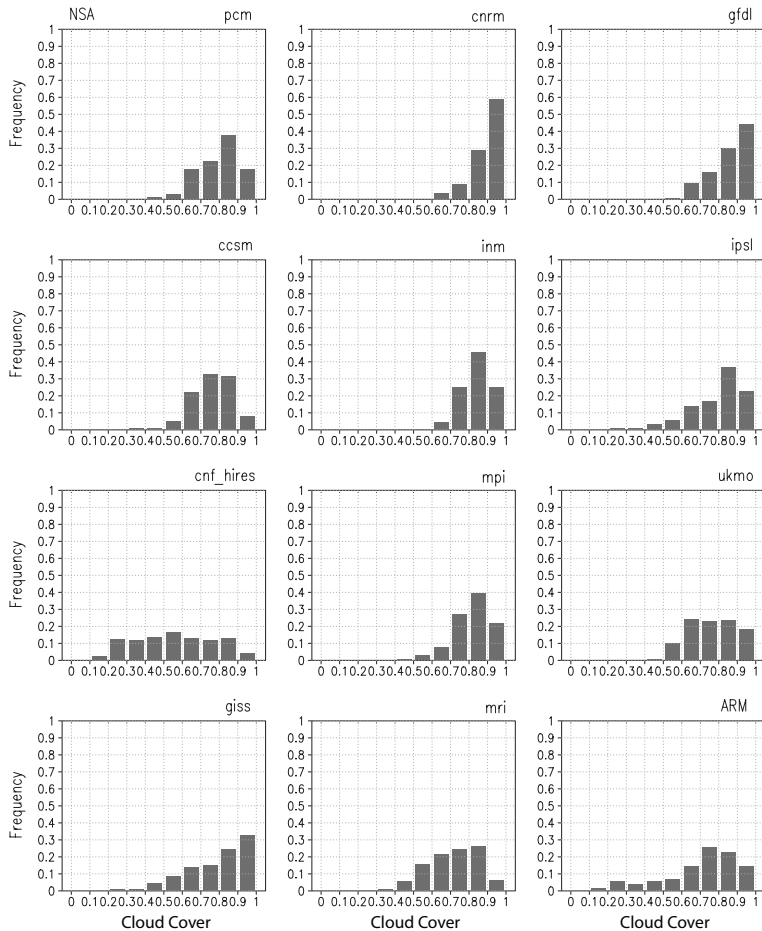


Fig. 7c. Continued.

Evaluation of cloud fraction and its radiative effect

Y. Qian et al.

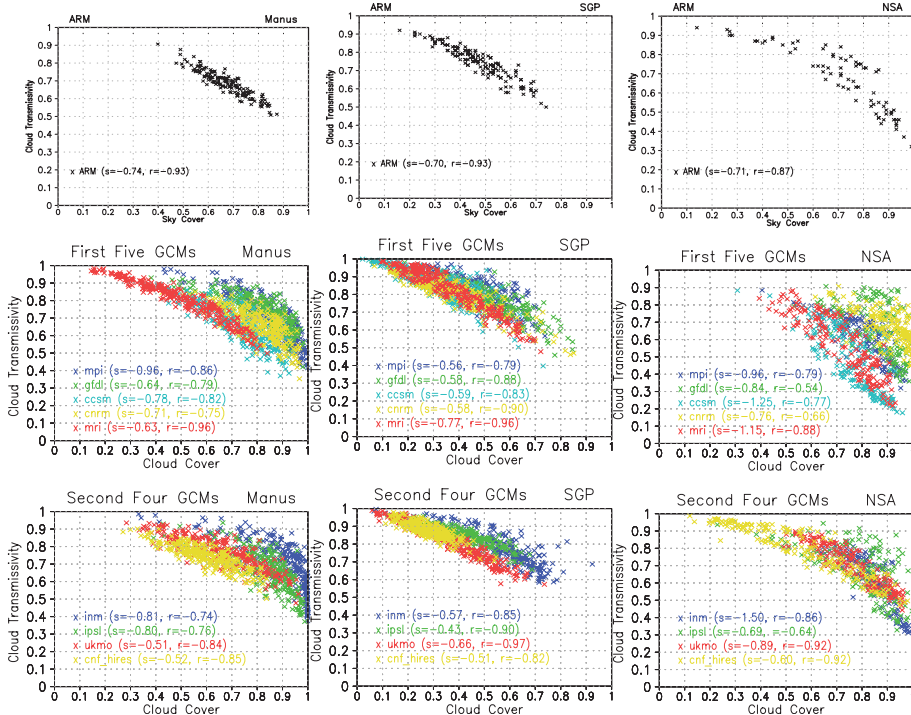


Fig. 8. The monthly mean SW transmissivity (T_{sw}) against their corresponding TCF for both observation and nine GCMs over three ARM sites. **(a)** Manus, **(b)** SGP, and **(c)** NSA.

Evaluation of cloud fraction and its radiative effect

Y. Qian et al.

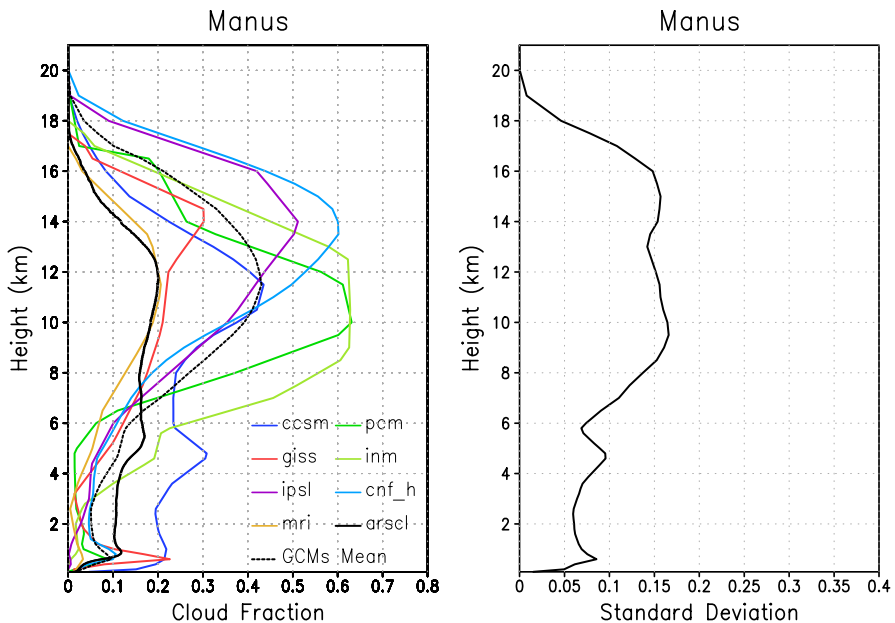


Fig. 9. The annual mean vertical profiles of cloud fraction (CF) from ARSCL observation and GCMs over Manus.

Evaluation of cloud fraction and its radiative effect

Y. Qian et al.

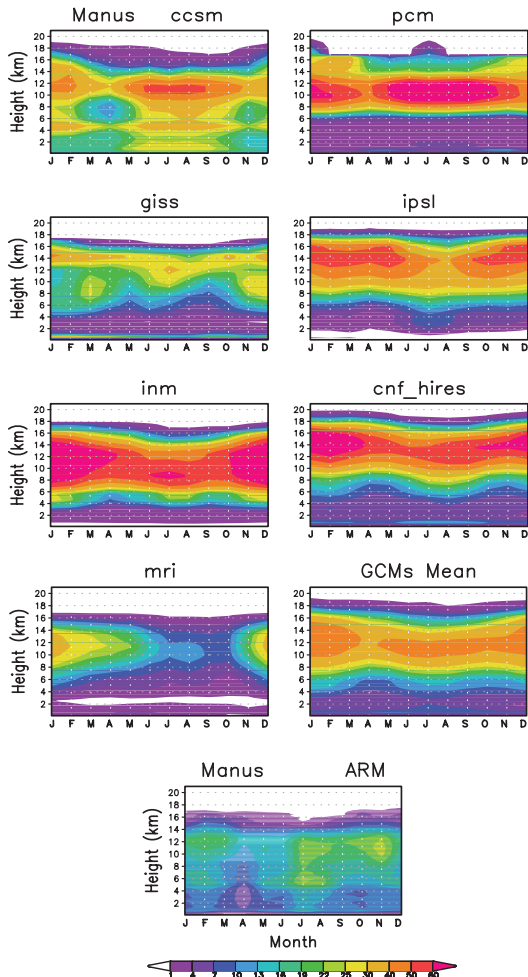
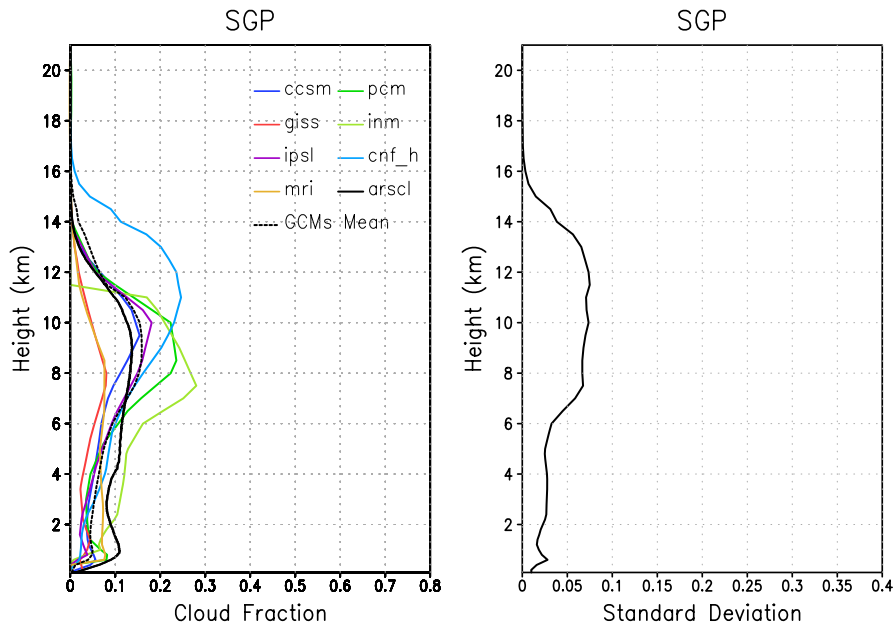


Fig. 10. The monthly mean time-height plots of cloud fraction (CF) from ARSCL observation and GCMs over Manus.

Evaluation of cloud fraction and its radiative effect

Y. Qian et al.

**Fig. 11.** Same as for Fig. 9, but for SGP.

- [Title Page](#)
- [Abstract](#) [Introduction](#)
- [Conclusions](#) [References](#)
- [Tables](#) [Figures](#)
- [◀](#) [▶](#)
- [◀](#) [▶](#)
- [Back](#) [Close](#)
- [Full Screen / Esc](#)
- [Printer-friendly Version](#)
- [Interactive Discussion](#)



Evaluation of cloud fraction and its radiative effect

Y. Qian et al.

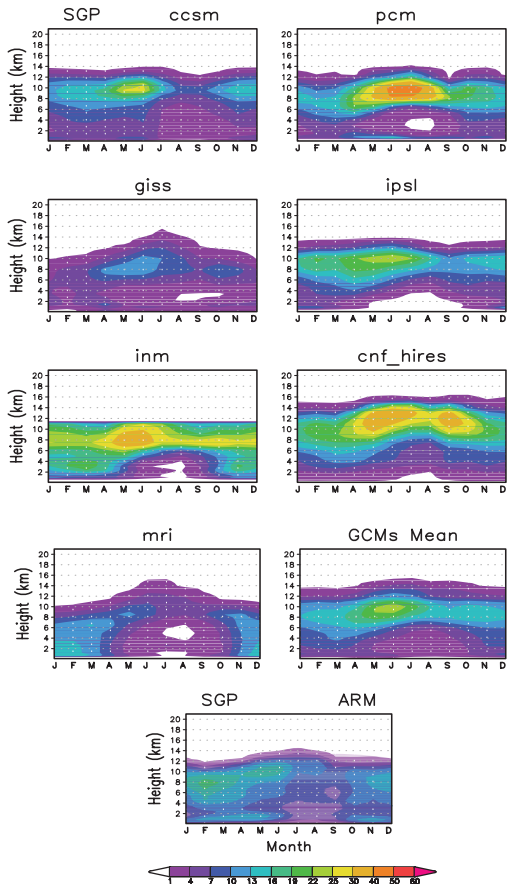
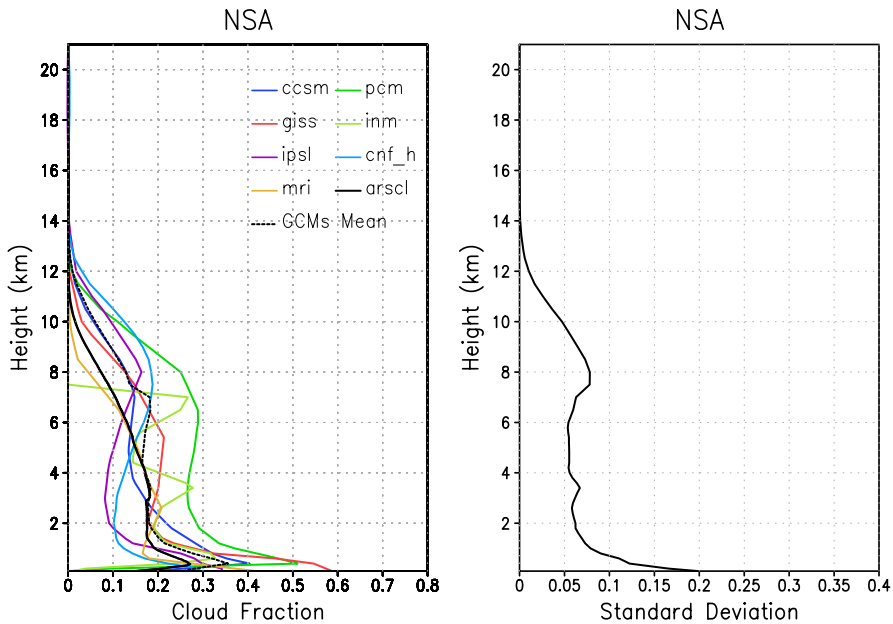


Fig. 12. Same as for Fig. 10, but for SGP.

Evaluation of cloud fraction and its radiative effect

Y. Qian et al.

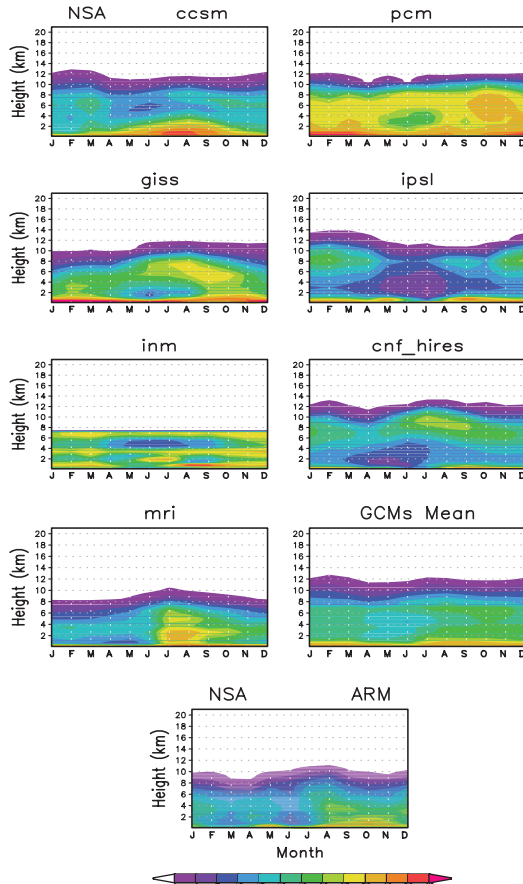
**Fig. 13.** Same as for Fig. 9, but for NSA.

- [Title Page](#)
- [Abstract](#) [Introduction](#)
- [Conclusions](#) [References](#)
- [Tables](#) [Figures](#)
- [◀](#) [▶](#)
- [◀](#) [▶](#)
- [Back](#) [Close](#)
- [Full Screen / Esc](#)
- [Printer-friendly Version](#)
- [Interactive Discussion](#)



Evaluation of cloud fraction and its radiative effect

Y. Qian et al.

**Fig. 14.** Same as for Fig. 10, but for NSA.

Evaluation of cloud fraction and its radiative effect

Y. Qian et al.

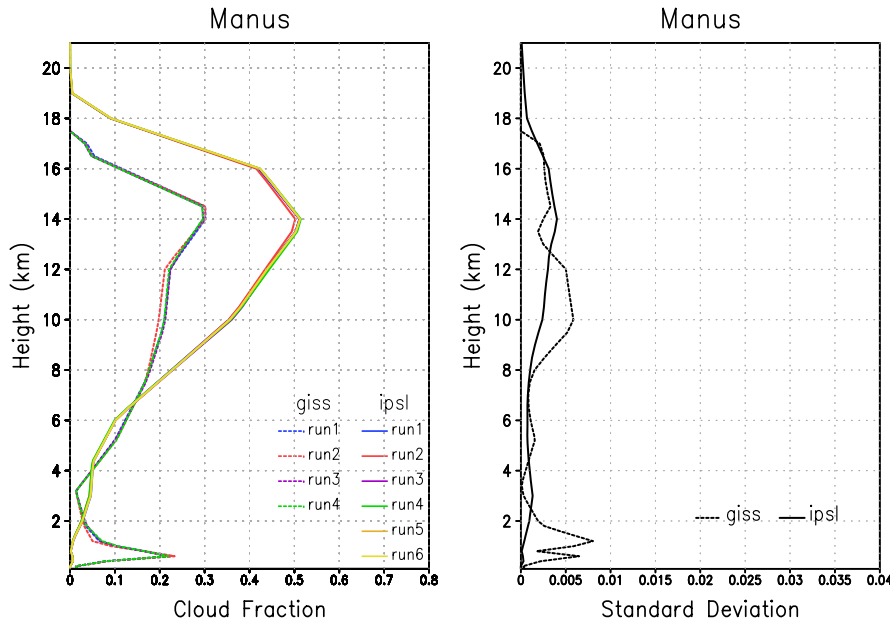


Fig. 15. The vertical profiles of cloud fraction (CF) for four GISS and six IPSL simulations (left), and their standard deviations (SD, right) among ensemble runs over Manus.

Title Page	
Abstract	Introduction
Conclusions	References
Tables	Figures
	
	
Back	Close
Full Screen / Esc	
Printer-friendly Version	
Interactive Discussion	